© 2014. Published by The Company of Biologists Ltd | Journal of Cell Science (2014) 127, 3505–3520 doi:10.1242/jcs.149112

RESEARCH ARTICLE

Phosphorylation of nucleoporin Tpr governs its differential localization and is required for its mitotic function

Kalpana Rajanala, Anshuk Sarkar, Gagan Deep Jhingan, Raina Priyadarshini, Manisha Jalan, Sagar Sengupta and Vinay Kumar Nandicoori*

ABSTRACT

A major constituent of the nuclear basket region of the nuclear pore complex (NPC), nucleoporin Tpr, plays roles in regulating multiple important processes. We have previously established that Tpr is phosphorylated in both a MAP-kinase-dependent and MAP-kinase-independent manner, and that Tpr acts as both a substrate and as a scaffold for ERK2 (also known as MAPK1). Here, we report the identification of S2059 and S2094 as the major novel ERK-independent phosphorylation sites and T1677, S2020, S2023 and S2034 as additional ERK-independent phosphorylation sites found in the Tpr protein *in vivo*. Our results suggest that protein kinase A phosphorylates the S2094 residue and that the site is hyperphosphorylated during mitosis. Furthermore, we find that Tpr is phosphorylated at the S2059 residue by CDK1 and the phosphorylated form distinctly localizes with chromatin during telophase. Abrogation of S2059 phosphorylation abolishes the interaction of Tpr with Mad1, thus compromising the localization of both Mad1 and Mad2 proteins, resulting in cell cycle defects. The identification of novel phosphorylation sites on Tpr and the observations presented in this study allow better understanding of Tpr functions.

KEY WORDS: Phosphorylation, Nucleoporin Tpr, Mitosis, Localization

INTRODUCTION

Nucleoporins are vital components of the nuclear envelope that mediate several crucial cellular processes, such as the transport of macromolecules, progression of the cell cycle, gene expression and chromatin organization. Over the past decade, the phosphorylation of nucleoporins has been shown to serve as a means to transduce cellular signals for the regulation of crucial functions such as nucleocytoplasmic transport and cell cycle progression (Kosako and Imamoto, 2010; Makhnevych et al., 2003; Schneider and Grosschedl, 2007; Yoon et al., 2008). Many cellular kinases, namely CDK1, ERK2 (also known as MAPK1) and protein kinases A and C have been reported to phosphorylate nucleoporins (Cai et al., 2002; De Souza et al., 2004; Eblen et al., 2003; Kosako et al., 2009; Lusk et al., 2007; Macaulay et al., 1995; Miller et al., 1999; Mühlhäusser and Kutay, 2007; Onischenko et al., 2005; Wu et al., 1995). Phosphorylation of the FG-repeat-containing nucleoporins (FG-Nups) Nup153 and Nup214 has been shown to disrupt their interaction with importin-β, thus inhibiting the import of nuclear proteins (Kosako et al., 2009).

In addition, nucleoporins have been shown to be extensively phosphorylated during mitosis both *in vitro* and *in vivo* (Blethrow et al., 2008; Bodoor et al., 1999; Favreau et al., 1996; Glavy et al., 2007; Macaulay et al., 1995; Mansfeld et al., 2006; Nousiainen et al., 2006). Mitotic phosphorylation of Nup50 and other FG-Nups has been shown to be crucial for the organization of spindle microtubules and chromosomes (Clarke and Bachant, 2008; Harel and Forbes, 2004; Hetzer et al., 2002; Tahara et al., 2008). Although these studies provide evidence that phosphorylation of nucleoporins is likely to modulate several physiological functions, the spatio-temporal regulation of these phosphorylation events and their influence on nuclear transport and/or regulation of mitotic functions have not yet been deciphered.

Nucleoporin Tpr, which is associated with the nuclear basket region, was initially thought to function as a scaffolding element, regulating intranuclear and nucleocytoplasmic transport at the nuclear phase of the nuclear pore complex (NPC) (Fontoura et al., 2001; Frosst et al., 2002; Shibata et al., 2002; Zimowska and Paddy, 2002). However, in the recent past, Tpr has been shown to play crucial roles in modulating other diverse cellular functions. Tpr associates with Mad1, Mad2 and the members of the dynein complex during mitosis, and these interactions have been found to be crucial for mediating the proper segregation of chromosomes during anaphase (Lee et al., 2008; Lince-Faria et al., 2009; Nakano et al., 2010). Tpr has also been shown to be required for establishing heterochromatin exclusion zones (HEZs) (Krull et al., 2010). Although Tpr has a limited role in modulating nucleocytoplamic transport of processed mRNA and proteins, it has been shown to regulate constitutive transport element (CTE)-dependent unspliced RNA export (Coyle et al., 2011; Rajanala and Nandicoori, 2012). Depletion of Tpr also results in enhanced p53 accumulation in the cell nucleus, resulting in a senescence-like phenotype and facilitating autophagy (David-Watine, 2011; Funasaka et al., 2012). Recently, Tpr was shown to be required for maintaining the homeostasis of Mad proteins and for the normal spindle assembly checkpoint response (Schweizer et al., 2013). We undertook the present study with the aim of investigating the phosphorylation status of the Tpr protein and the significance of specific Tpr phosphorylation events during cell cycle progression. We demonstrate that the phosphorylation of Tpr is crucial for the regulation of differential localization of the protein and for normal Tpr function during mitosis.

National Institute of Immunology, Aruna Asaf Ali Marg, New Delhi 110 067, India.

*Author for correspondence (vinaykn@nii.ac.in)

Received 6 January 2014; Accepted 5 June 2014

Journal of Cell Science (2014) 127, 3505–3520 doi:10.1242/jcs.149112

RESULTS

Tpr is phosphorylated at residues S2059 and S2094 *in vivo*

Tpr has previously been shown to be phosphorylated by the MAP kinase ERK2 (Eblen et al., 2003). Phosphorylated Tpr acts as both a substrate and a scaffold for ERK2 at the NPC, allowing ERK2 to phosphorylate proteins that interact with Tpr (Vomastek et al., 2008). Previously, we have shown that phosphopeptide maps obtained for the metabolically labeled full-length and carboxy-terminal fragment of Tpr were identical (Vomastek et al., 2008), which suggested that both ERK2-dependent and ERK2-independent phosphorylation sites are present in the carboxy-terminal 800 amino acids. Because the sites of ERK2-mediated phosphorylation were already mapped, we set out to identify the ERK2-independent phosphorylation sites in Tpr. Accordingly, the carboxy-terminal fragment of Tpr protein (TprC) and TprC-M4, wherein all ERK2 target sites have been mutated to alanine (Fig. 1A), were metabolically labeled. Autoradiography showed a prominent band at the position of Tpr (Fig. 1B), indicating robust phosphorylation. Whereas ERK2-mediated phosphorylation disappeared in tryptic phosphopeptide maps of TprC-M4 (Fig. 1C, dotted circle), we observed the presence of three spots resulting from ERK-independent phosphorylation in both maps (Fig. 1C; indicated by arrows). The phospho-amino-acid analysis revealed that the ERK-independent phosphorylation events mainly affected serine residues (Fig. 1D). In order to narrow down the target phosphorylation regions, we created a series of nested deletions from both ends of TprC-M4 (supplementary material Fig. S1A). All of these fragments were metabolically labeled, and five out of the six proteins so created had the same phosphopeptide map as TprC-M4. However, in the case of TprC-ΔC3, all three spots corresponding to ERK-independent phosphorylation disappeared (supplementary material Fig. S1B, missing spots are indicated). Thus, major ERK-independent phosphorylation events are likely to occur within the 117-amino-acid stretch between residues 2029 and 2146 of Tpr. Based on the phospho-amino-acid analysis (Fig. 1C) and computational analysis of the 117-amino acid stretch using Scansite (Obenauer et al., 2003), we analyzed the likely phosphorylation of specific serine residues in three putative target tryptic peptides. Although the peptide map for the combinatorial triple mutant TprC-M4-(S2046, 2047, 2049A) was similar to that of the wild-type peptide, peptide maps of

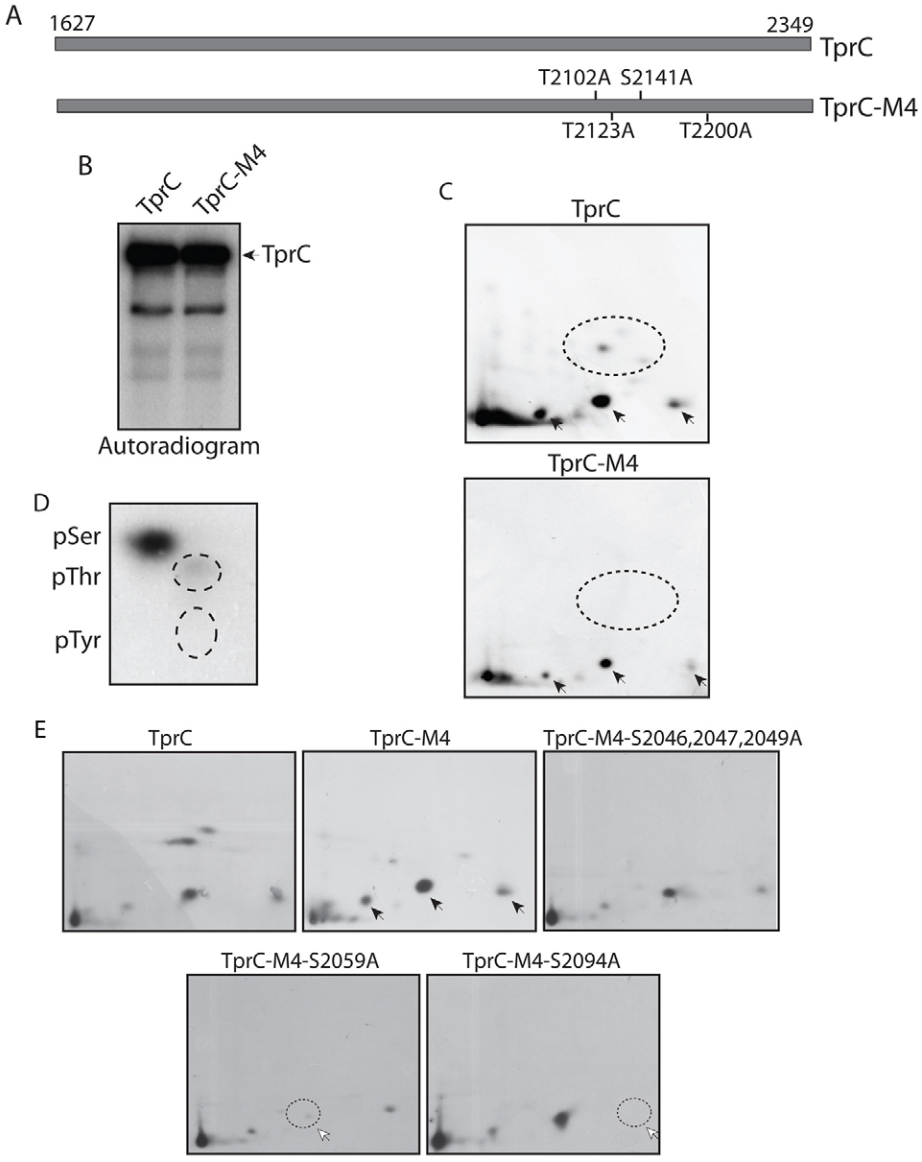

Fig. 1. Nucleoporin Tpr is phosphorylated *in vivo* at residues S2059 and S2094. (A) Schematic representation of the TprC and TprC-M4 constructs. (B) COS-1 cells transfected with constructs encoding FLAG–TprC or FLAG–TprC-M4 were metabolically labeled, and FLAG-tagged proteins were immunoprecipitated, resolved and autoradiographed. (C) *In-vivo*-labeled TprC and TprC-M4 were digested with trypsin, and the resulting phosphopeptides were mapped by 2D thin-layer chromatography (TLC). Arrows indicate the labeled phosphopeptides that were persistent in the *in vivo* map of TprC-M4. Dotted circles indicate ERK2-mediated phosphorylation, which is lost from TprC-M4. (D) Phospho-amino-acid analysis of the labeled TprC-M4 protein. The dotted circles show the migration of phosphorylated threonine (pThr) and phosphorylated tyrosine (pTyr) amino acid standards detected by ninhydrin staining. (E) Metabolically labeled TprC-M4-(S2046,2047,2049A), TprC-M4-(S2059A) and TprC-M4-(S2094A) proteins were digested with trypsin and were mapped by 2D-TLC. White arrows and dotted circles indicate the disappearance of labeled phosphopeptide spots that are indicated with black arrows for TrpC-M4.

TprC-M4-(S2059A) and TprC-M4-(S2094A) showed the absence of specific radiolabeled spots (Fig. 1E, dotted circles). These results clearly demonstrate that Tpr is phosphorylated at the residues S2059 and S2094 *in vivo*.

Minor phosphorylation of Tpr at T1677, S2020, S2023 and S2034 residues

In order to determine the stoichiometry of phosphorylation on S2059 and S2094 residues, we resorted to high-resolution mass spectrometry analysis of immunoprecipitated FLAG–TprC-M4. Liquid chromatography-mass spectrometry (LC-MS) analyses showed the presence of two phosphopeptides with precursor mass-to-charge ratio (m/z) of 815.746 and 856.01, corresponding to the mass of triply charged tryptic phosphopeptides from residues 1657–1680 and 2016–2041, respectively. Tandem mass spectrometry (MS/MS) analysis of these two precursors unambiguously identified T1677 and S2034 to be the target phosphorylation sites (Fig. 2A,C). In addition, analysis also showed the presence of a triply charged precursor (m/z 882.67) corresponding to dually phosphorylated tryptic peptide from residues 2016–2041, and a quadruply charged precursor (m/z 781.86) corresponding to the singly phosphorylated semi-tryptic peptide from residues 2092–2118. MS/MS analysis identified S2020 and S2023 on dually phosphorylated peptide, and S2094 on semi-tryptic peptide, to be the target sites of phosphorylation (Fig. 2B,D). However, we could not detect any precursor phosphopeptide containing the major site of phosphorylation, S2059. The quantity of a peptide in a high-resolution mass spectrometry analysis can be determined by calculating the sum of its isotopic peak area at the MS1 level. To determine the stoichiometry of phosphorylation, we utilized the Precursor Ions Area Detector Node to determine the area of peaks corresponding to phosphopeptides and their unphosphorylated counterparts. Based on this analysis, phosphorylation of T1677, S2020, S2023 and S2034 residues ranges from ~0.6% to 2.7% (Fig. 2G), thus demonstrating that these are minor phosphorylation sites on Tpr. By contrast, phosphorylation on S2094 is relatively more abundant, with 9% of protein being phosphorylated at this residue (Fig. 2G). Because the tryptic peptide containing the S2059 site could not be detected by mass spectrometry, we resorted to two-dimensional (2D) gel electrophoresis to determine the abundance of S2059 phosphorylation. A shift in protein migration towards the acidic end of the immobilized pH gradient (IPG) strip might sometimes occur owing to the negatively charged phosphate group. Western blot analysis detected two spots of Tpr for TprC-M4 and TprC-M4-S2094A (Fig. 2F, indicated by arrow), but only one spot for TprC-M4-S2059A (missing spot indicated by circle), suggesting that S2059 is a phosphorylation site. The spot intensities, as calculated by using ImageJ software, indicated that ~10% of TprC protein was phosphorylated at the S2059 residue. Analysis of the Tpr primary sequence using Scansite at low stringency predicted multiple kinases capable of phosphorylating the above sites (Fig. 2G). Taken together, using peptide maps, high resolution mass spectrometry and 2D gels, we have identified S2059 and S2094 to be the major ERK-independent phosphorylation sites and T1677, S2020, S2023 and S2034 to be minor ERK-independent phosphorylation sites on Tpr (Fig. 2E).

Phosphospecific antibodies specifically recognize phosphorylation on S2059 and S2094

To examine the role of S2059 and S2094 phosphorylation in Tpr functions, we raised phosphospecific antibodies. The specificity and sensitivity of Tpr-pS2059 and pS2094 antibodies were checked by probing either His–TprC that was purified from bacteria or cell lysates that were isolated from COS-1 cells expressing FLAG-tagged TprC, TprC-S2059A and TprC-S2094A (Fig. 3A,B). Although both His–TprC purified from bacteria and FLAG–TprC proteins expressed in COS-1 cells could be efficiently detected by antibodies against Tpr, anti-Tpr-pS2059 and anti-Tpr-pS2094 antibodies could only detect FLAG–TprC that was expressed in COS-1 cells (Fig. 3A,B). The inability of antibodies against Tpr-p2059 and Tpr-pS2094 to detect His–TprC expressed in bacteria and either FLAG-tagged S2059A or S2094A mutants, respectively, demonstrates the ability of these antibodies to specifically detect phosphorylated Tpr (Fig. 3A,B). Western blot analysis of cell lysates from COS-1 cells transfected with full-length FLAG–Tpr-Si (a construct encoding an siRNA-resistant version of Tpr; Rajanala and Nandicoori, 2012), or FLAG–Tpr-Si-2059A or FLAG–Tpr-Si-S2094A mutants, revealed that antibodies against Tpr-pS2059 and Tpr-pS2094 have the ability to specifically detect full-length phosphorylated Tpr proteins (Fig. 3C,D). We then analyzed the ability of these antibodies to detect the phosphorylated Tpr protein by immunofluorescence microscopy. Although we observed classical nucleoporin-rim staining using antibodies against Tpr and Tpr-pS2059 (Fig. 3E), only ~40% cells showed clear rim staining when probed with antibody against Tpr-pS2094 (Fig. 3E). In the remaining cell population, we reproducibly observed diminished rim staining, suggesting that Tpr phosphorylated on S2094 either shows altered localization or is degraded (Fig. 3E). In addition to classical rim staining, anti-Tpr-pS2059 antibodies could also detect Tpr in the nucleoplasmic fraction (Fig. 3E). In order to determine the ability of phosphospecific antibodies to specifically detect the phosphorylation of endogenous Tpr, western blots were performed with the cell lysates prepared from HeLa cells transfected with non-specific (NS)-siRNA or Tpr-specific siRNA. Lysates from Tpr-siRNA-transfected HeLa cells showed a significant reduction in Tpr protein levels and, concomitantly, in the levels of Tpr phosphorylated at S2059 and S2094 (Fig. 3F). To establish whether the immunofluorescence staining obtained by using the phosphospecific antibodies is specific for the Tpr protein, HeLa cells were transfected with Tpr-siRNA and the cells were stained with antibodies against Tpr, Tpr-pS2059 and Tpr-pS2094. We observed diminished rim staining in Tpr-depleted cells when using the anti-Tpr antibody. A corresponding decrease could also be seen with the antibodies against Tpr-pS2059 and Tpr-pS2094 (Fig. 3G), thus reaffirming the specificity of the antibodies.

PKA and CDK1 phosphorylate Tpr at the S2094 and S2059 residues, respectively

Analysis of the primary amino acid sequence of Tpr using Scansite at high stringency suggested that S2094 might be a target for protein kinase A (PKA). To test this, kinase assays were performed by incubating immunoprecipitated PKA or HA–ERK2 with immunoprecipitated FLAG–TprC, TprC-S2059A or TprC-S2094A. In agreement with the previous data (Vomastek et al., 2008), we detected strong phosphorylation of TprC by ERK2 (Fig. 4A, left panel). Although we observed robust phosphorylation of TprC and TprC-S2059A by PKA, phosphorylation of the TprC-S2094A mutant by PKA was almost negligible, indicating that S2094 is indeed a PKA target *in vitro* (Fig. 4A, right panel). Peptide-map analysis of ERK2-mediated Tpr phosphorylation showed tryptic peptide spots at previously identified positions

Journal of Cell Science (2014) 127, 3505–3520 doi:10.1242/jcs.149112

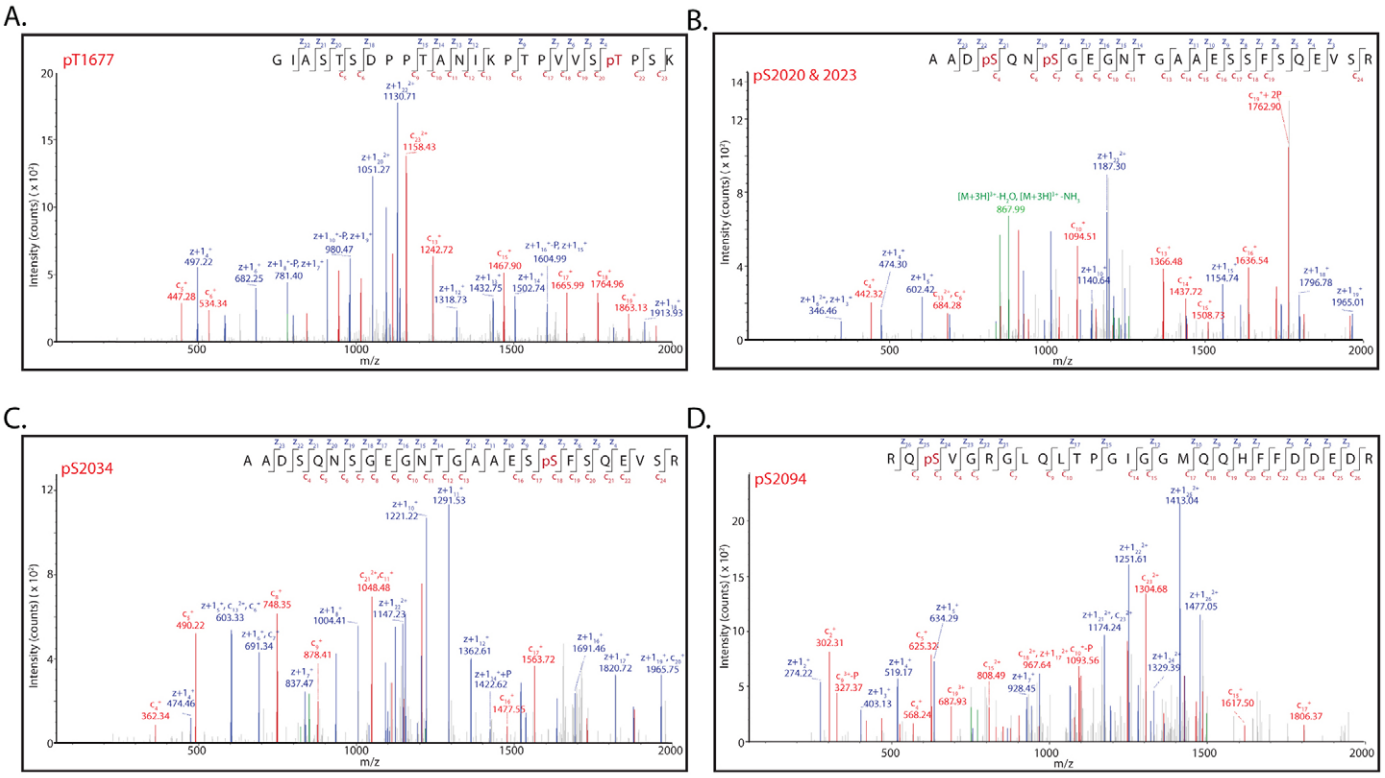

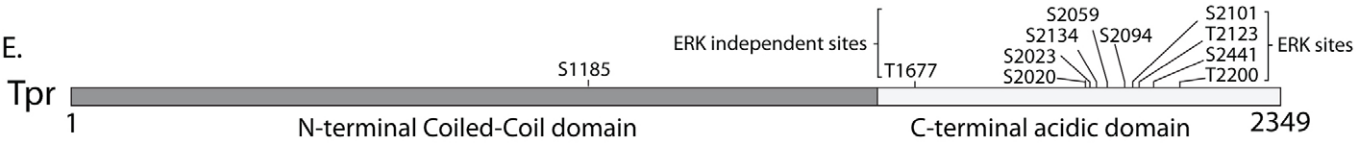

F.

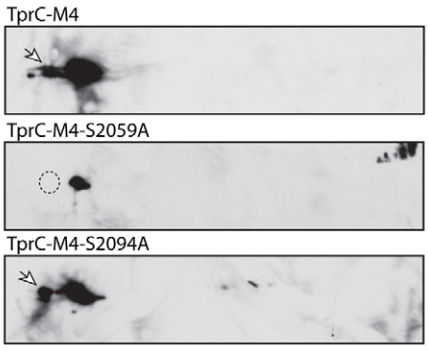

G.

S. No	Peptide sequence	Identification method	Site	Stoichiometry of phosphorylation	Probable Kinases
1	[1657]GIASTSDPPTANIKPTPVVS**pT**PSK[1680]	Mass spec	T1677	0.64%	Cdk1 motif
2	[2016]AAD**pS**QN**pS**GEGNTGAAESSFSQEVSR[2041]	Mass spec	S2020 S2023	0.69%	DNA PK, ATM kinase
3	[2016]AADSQNSGEGNTGAAES**pS**FSQEVSR[2041]	Mass spec	S2034	2.69%	Casine kinase 2, PLK1 kinase
4	[2056]APQ**pS**PR[2051]	Peptide map	S2059	10%	CDK1 motif, Cdc2 kinase, Cdk5 kinase, p38 MAPK, GSK3 kinase
5	[2092]RQ**pS**VGRGLQLTPGIGGMQQHFFDDEDR[2119]	Mass spec & Peptide map	S2094	9.01%	Aurora A, Aurora B, Protein Kinase A

Fig. 2. Identification of phosphorylation sites by mass spectrometry. (A–D) LC-MS/MS data showing electron transfer dissociation (ETD)-induced fragmentation mass spectra identifying four phosphopeptides in Tpr. pT and pS indicates the site of phosphorylation. (A) MS/MS spectrum of precursor *m/z 815.74695* (+3) and MH^+ 2445.22629 Da, of the semi-tryptic phosphopeptide GIASTSDPPTANIKPTPVVS(pT)PSK. The unambiguous location of the intact phosphate group on T1677 was determined by the presence of the 'C' and 'Z' ion series containing C_{22}, C_{23} and $Z_{4–7}$, Z_9, $Z_{12–15}$, Z_{18} and $Z_{20–22}$. (B) MS/MS spectrum of precursor *m/z 882.67010* (+3) and MH^+ 2645.99576 Da, of the phosphopeptide AAD(pS)QN (pS)GEGNTGAAESSFSQEVSR. The location of the intact phosphate groups was confirmed by the observation of the 'C' and 'Z' ion series containing C_4, $C_{6–11}$, $C_{13–19}$, C_{24} and Z_{19} and $Z_{21–23}$. (C) MS/MS spectrum of precursor *m/z 856.01892* (+3) and MH^+ 2566.04221 Da, of phosphopeptide AADSQNSGEGNTGAAES(pS)FSQEVSR. The location of S2034 was evident by the observation of the ion series containing $C_{18–22}$, C_{24} and $Z_{8–12}$ and $Z_{14–23}$. (D) MS/MS spectrum of precursor *m/z 781.86627* (+4) and MH^+ 3124.44326 Da, of semi-tryptic phosphopeptide RQ(pS)VGRGLQLTPGIGGMQQHFFDDEDR. The presence of a phosphate group at S2094 is confirmed by the appearance of the ion series containing $C_{3–5}$, C_7, $C_{9–10}$, $C_{14–15}$, $C_{17–26}$ and $Z_{25–26}$. (E) A schematic outline indicating all the phosphorylation sites on Tpr. The S1185 residue was identified to be a target for PLK1 (Santamaria et al., 2011) (F) FLAG-tagged wild-type and mutant TprC-M4 proteins were resolved on 13-cm pH 3.5–5.6 non-linear gradient IPG strips for 25,000 Vh. IPG strips were resolved in the second dimension by SDS-PAGE on 10% gels, transferred to nitrocellulose membrane and subjected to western blotting with mouse anti-FLAG antibodies. The arrows show the spot corresponding to Tpr phosphorylated at S2059; the dotted circle shows the disappearance of this spot in the phospho-mutant TprC-M4-S2059A. (G) Compilation of all the data for the identified sites. The stoichiometry of phosphorylation for sites identified by mass spectrometry were determined as described in Materials and Methods. To determine the stoichiometry of phosphorylated S2059 species, we used ImageJ quantification (Schneider et al., 2012) of the 2D gels presented in F. Probable kinase prediction was performed using Scansite software and the search was performed at low stringency (Obenauer et al., 2003). Phosphorylated amino acids are shown in red.

Journal of Cell Science (2014) 127, 3505–3520 doi:10.1242/jcs.149112

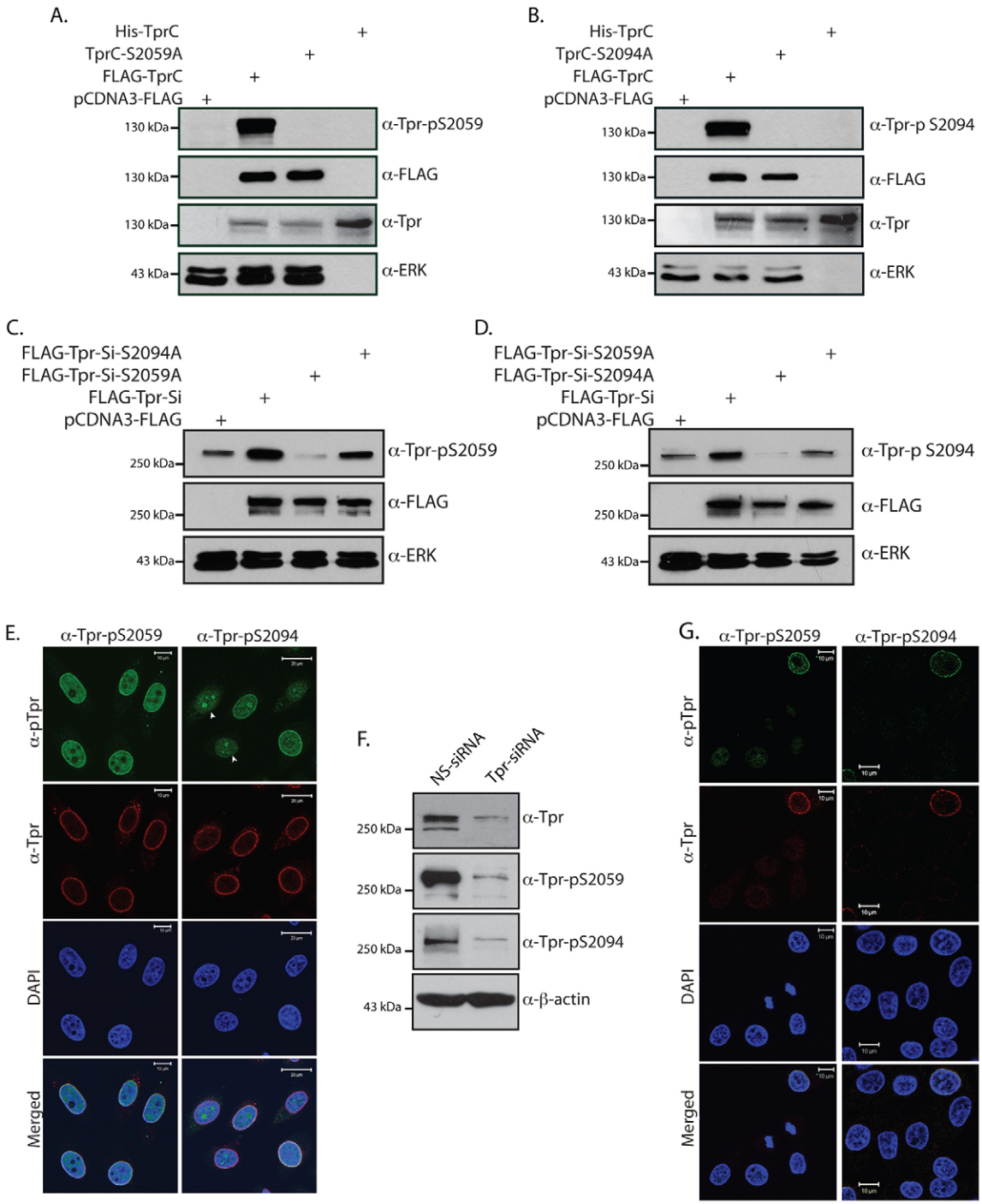

Fig. 3. Characterization of phosphospecific antibodies of Tpr. (A,B) COS-1 cells were transfected with 2 μg each of pCDNA3-FLAG construct or constructs encoding FLAG–TprC, FLAG–TprC-S2059A or FLAG–TprC-S2094A. The lysates obtained at 36 h after transfection were loaded alongside the purified bacterial TprC protein. The samples were resolved and transferred onto nitrocellulose membrane, and the blot was probed with anti-FLAG, anti-ERK, rabbit polyclonal anti-Tpr (Frosst et al., 2002) anti-Tpr-pS2059 and anti-Tpr-pS2059 antibodies. (C,D) COS-1 cells were transfected with 2 μg each of pCDNA3-FLAG construct or constructs encoding FLAG–Tpr-Si, FLAG–Tpr-Si-S2059A or FLAG–Tpr-Si-S2094A. The lysates were then analyzed with anti-FLAG, anti-ERK, anti-Tpr-pS2059 and anti-Tpr-pS2059 antibodies. (E) Immunofluorescence analysis of HeLa cells stained with anti-Tpr (red), anti-Tpr-pS2059 (green) and anti-Tpr-pS2094 (green) antibodies. Arrowheads show the nucleolar localization of Tpr-pS2094. Scale bars: 10 μm (left panels), 20 μm (right panels). (F) HeLa cells were transfected with non-specific siRNA (NS-siRNA) or Tpr-specific siRNA (Tpr-siRNA). At 48 h post-transfection, the cell lysates were probed with mouse monoclonal anti-Tpr (Abcam), anti-β-actin, anti-Tpr-pS2059 and anti-Tpr-pS2094 antibodies. (G) Immunofluorescence analysis of HeLa cells transfected with Tpr-specific siRNA and stained with anti-Tpr-pS2059 (green) or anti-Tpr-pS2094 (green) and anti-Tpr (red) antibodies. Scale bars: 10 μm.

(Fig. 4B, dotted ellipse). Analysis of PKA-mediated Tpr phosphorylation showed only one tryptic peptide spot, spot 3, corresponding to S2094. To establish whether S2094 is a bona fide *in vivo* target of PKA, HeLa cells were transfected with either NS-siRNA or PKA-specific siRNA, and cell lysates were probed with the phosphospecific antibodies. As expected, the phosphorylation of

Journal of Cell Science

Journal of Cell Science (2014) 127, 3505–3520 doi:10.1242/jcs.149112

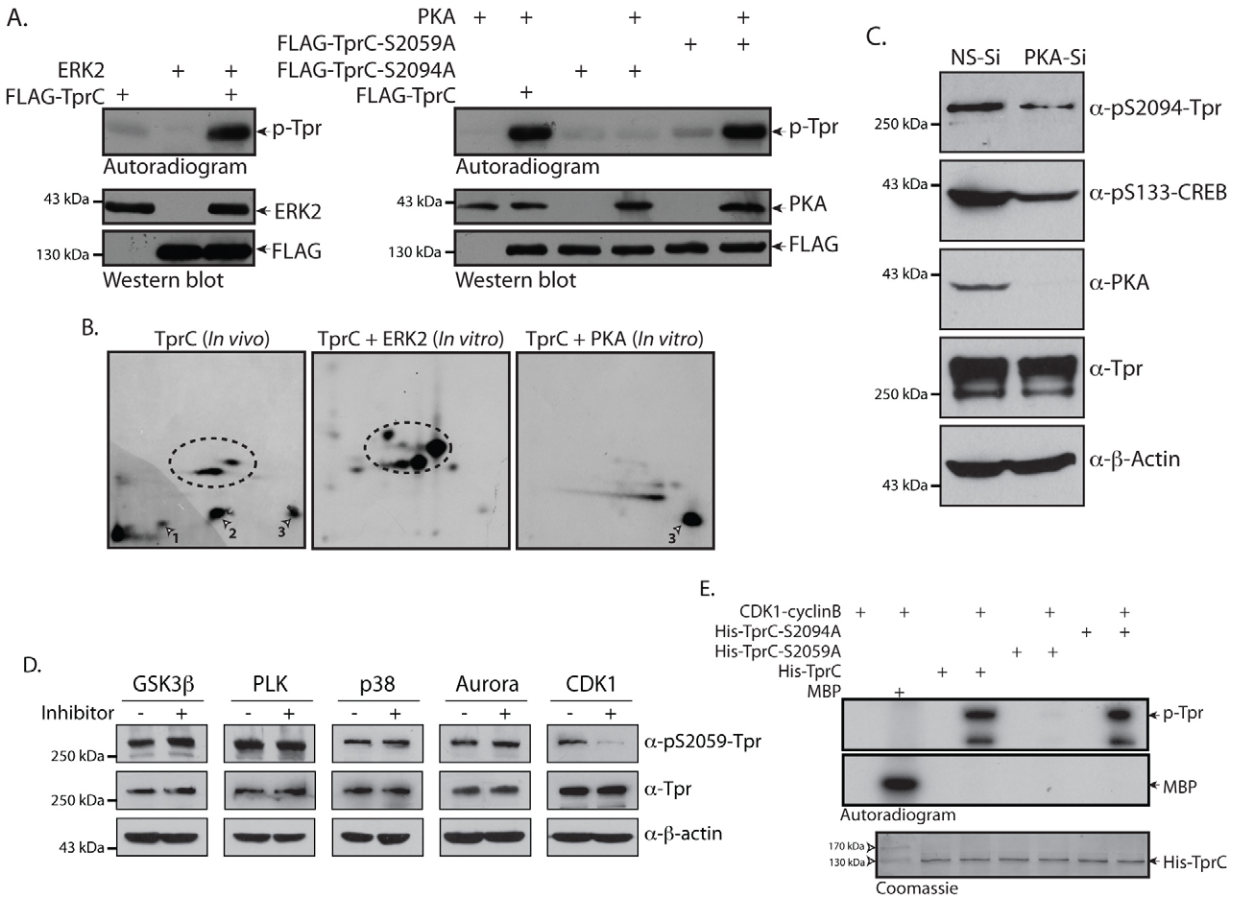

Fig. 4. PKA and CDK1 phosphorylate Tpr at residues S2094 and S2059, respectively. (A) COS-1 cells were transfected with 8 μg each of constructs encoding wild-type FLAG–TprC, FLAG–TprC-S2059A, FLAG–TprC-S2094A, HA–ERK2 and CMV-PKA. The lysates of cell obtained at 36 h post-transfection were immunoprecipitated with anti-FLAG, anti-HA or anti-PKA antibodies. The immunoprecipitated FLAG–TprC or CMV-PKA were mixed either with immunoprecipitated HA–ERK2 or with FLAG–TprC, FLAG–TprC-S2059A or FLAG–TprC-S2094A samples, respectively, and kinase reactions were performed in the presence of [γ-^{32}P]-ATP at 30°C for 10 min. (B) TprC phosphorylated *in vitro* by either ERK2 or PKA was digested with trypsin, and the resulting phosphopeptides were mapped by 2D-TLC. A comparative peptide map of the *in-vivo*-labeled TprC protein is also shown. Arrowheads show the ERK-independent tryptic phosphopeptides; dotted circles show ERK-mediated phosphorylation. (C) COS-1 cells were transfected with either NS-siRNA (NS-Si) or PKA-specific siRNA (PKA-Si) and, 96 h post-transfection, cell lysates were probed with anti-PKA, anti-β-actin, anti-CREB-pS133, anti-Tpr and anti-Tpr-pS2094 antibodies. (D) HeLa cells were treated with inhibitors against GSK3β (Inhibitor VIII; 10 μM), PLK (BI2536; 100 nM), p38 (SB203580; 20 μM), Aurora kinase (MLN8237; 500 nM) and CDK1 (RO3306; 10 μM) for 2 h. Cells were lysed in 2× SDS sample buffer and the lysates were then probed with anti-Tpr, anti-Tpr-pS2059 and anti-β-actin antibodies. (E) Wild-type His–TprC and the phospho-mutants His–TprC-S2059A and His–TprC-S2094A were purified from *E.coli*. The proteins were incubated with CDK1–cyclinB complex and kinase reactions were carried out in the presence of [γ-^{32}P]-ATP at 30°C for 10 min. The autoradiogram is shown, along with Coomassie Blue staining to visualize protein loading.

CREB, a known substrate of PKA, decreased upon PKA depletion (Fig. 4C). In agreement with the data presented in Fig. 4A,B, depletion of PKA resulted in decreased phosphorylation of the S2094 residue (Fig. 4C), thus verifying that the specific phosphorylation of Tpr on S2094 is dependent on PKA *in vivo*.

In order to identify the kinase phosphorylating the S2059 residue, we treated HeLa cells with inhibitors of different kinases, namely GSK3β, Polo-like kinase (PLK), p38, Aurora and CDK1. As evident from western blot analysis, the addition of inhibitors against GSK3β, PLK, p38 and Aurora kinases did not alter the phosphorylation status of S2059 (Fig. 4D). However, in the presence of CDK1 inhibitor (RO336), we observed a substantial decrease in the levels of S2059 phosphorylation (Fig. 4D). To validate these results, we performed *in vitro* kinase assays using purified His–TprC, His–TprC-S2059A and His–TprC-S2094A with CDK1–cyclinB. The results presented in Fig. 4E demonstrate that the complex was active, as was apparent from robust phosphorylation of universal substrate myelin basic protein (MBP). However, although the CDK1–cyclinB complex efficiently phosphorylated TprC and TprC-S2094A, the phosphorylation of TprC-S2059A was insignificant (Fig. 4E). Taken together, these data provide evidence that the phosphorylation of Tpr on S2059 is dependent on CDK1.

We have previously shown that although Tpr has a limited role in protein transport through the NPC, it specifically regulates the export of intron-containing RNA (Rajanala and Nandicoori, 2012). The role of Tpr in the export of unspliced RNA was investigated using well-characterized reporter constructs containing the coding sequences of human immunodeficiency virus (HIV) Gag/Pol proteins within an intron, followed by a CTE (Coyle et al., 2003). The levels of Gag protein in the cytoplasm, as quantified by enzyme-linked immunosorbent assay (ELISA) for p24, represents the extent of processed Gag protein (p24), a measure of export of intron-containing RNA. We sought to determine the impact of the phosphorylation of Tpr S2059 or S2094 residues on its role in modulating the export of unspliced

Journal of Cell Science (2014) 127, 3505–3520 doi:10.1242/jcs.149112

RNAs. In agreement with our previous data, depletion of Tpr resulted in elevated CTE-mediated export, which is indicated by elevated p24 levels in the cytosol (supplementary material Fig. S2A,B). As expected, restoration of Tpr protein levels by co-transfecting cells with siRNA-resistant Tpr-Si resulted in a significant reduction in p24 levels. The rescue of the phenotype observed with Tpr-Si-S2059A and Tpr-Si-S2094A mutants was similar to that observed with transfection of Tpr-Si (supplementary material Fig. 2A,B), suggesting that the phosphorylation of Tpr does not have any impact on the known transport function of Tpr.

Tpr protein levels and its phosphorylation are regulated during cell cycle

Several studies reported that nucleoporins are extensively phosphorylated during mitosis, and this mitotic-specific hyperphosphorylation has been demonstrated both *in vitro* and *in vivo* (Blethrow et al., 2008; Bodoor et al., 1999; Favreau et al., 1996; Glavy et al., 2007; Macaulay et al., 1995; Mansfeld et al., 2006; Nousiainen et al., 2006). We therefore sought to investigate the phosphorylation status of Tpr during the cell cycle and, specifically, during mitosis. To this end, HeLa cells were arrested at prometaphase by using nocodazole treatment, and mitotic cells obtained by 'shake off' were released from the nocodazole block into drug-free medium. Flow cytometry analysis confirmed the mitotic arrest at 0 h and the subsequent synchronized release of the cells into the G1 and S phases of cell cycle (Fig. 5A). Western blot analysis (Fig. 5B) suggested that the levels of Tpr are higher during mitosis than during interphase. The phosphorylation at S2059 correlated with Tpr expression levels, suggesting that the ratio of S2059-phosphorylated Tpr to total Tpr is not altered during cell cycle progression (Fig. 5B). By contrast, S2094 phosphorylation was considerably higher in mitotic cells and in the early stages of G1 (Fig. 5A,B).

The fact that we could observe the staining of all cells with an anti-Tpr-pS2059 antibody (Fig. 3E) and that the levels of S2059 phosphorylation are similar in the asynchronous and synchronised cell populations (Fig. 5B), clearly demonstrates that this represents a constitutive phosphorylation event on Tpr protein. Interestingly, when we immunostained the cells with antibody against Tpr-pS2094 to score for the cell-cycle-dependent phosphorylation at S2094 residue, we observed that certain cells exhibited distinctive nucleolar staining (Fig. 3E). In order to further confirm our findings, we performed immunofluorescence analysis with antibodies against Tpr-pS2094 and fibrillarin (nucleolus marker). The results suggested that, at certain stages of cell cycle, Tpr that is phosphorylated on S2094 localizes to the nucleolar compartment (Fig. 5C). In order to confirm the mitosis-specific hyperphosphorylation of the S2094 residue and to check the localization of S2094-phosphorylated Tpr during mitosis, immunofluorescence analysis of HeLa cells at different stages of mitosis was performed using antibodies against phosphorylated S2094. Upon microscopic examination of Tpr localization using antibodies against Tpr and Tpr-pS2094, we found that S2094-phosphorylated Tpr and total Tpr showed a similar distribution pattern through the different stages of mitosis (Fig. 5D).

Tpr phosphorylated at S2059 associates with chromatin during telophase

Tpr and its orthologs have been shown to be crucial for the progression of mitosis across different species (Lee et al., 2008; Lince-Faria et al., 2009; Nakano et al., 2010; Niepel et al., 2005). Immunofluorescence analysis using antibodies against Tpr and Tpr-pS2059 showed that the distribution of S2059-phosphorylated Tpr was the same as that of the Tpr protein during interphase and all the way up to metaphase (Fig. 6A). Interestingly, at anaphase and telophase, we observed that the localization of S2059-phosphorylated Tpr was different from that of unphosphorylated Tpr, with S2059-phosphorylated Tpr demonstrating a stronger staining near the segregating chromosomes in anaphase and a distinct pattern of colocalization with chromatin in telophase (Fig. 6A). A previous study has demonstrated that NPC components are sequentially reassembled at the pore after the completion of mitosis, and Tpr was shown to be one of the components that is recruited at the end of this process. It was speculated that Tpr might require an intact nuclear pore to allow the protein to traverse the nuclear membrane (Bodoor et al., 1999). Therefore, we sought to investigate the localization of Nup153 and FG-Nups during telophase, and we observed that although both the FG-Nups and Nup153 began associating with the nuclear membrane during telophase, both Tpr and S2059-phosphorylated Tpr were not recruited to the NPC at this stage (Fig. 6B; supplementary material Fig. S3A). These results are the first evidence of differential localization of a phosphorylated nucleoporin during mitosis.

Phosphorylation at the S2059 residue is required for the interaction of Tpr with Mad1 and the localization of Mad proteins

In our study, we observed significant phosphorylation of Tpr at both S2059 and S2094 residues during mitosis, a finding that suggests that these phosphorylation events might be crucial for mediating the known mitotic functions of Tpr. Mad1 and Mad2 proteins have been shown to regulate the mitotic spindle checkpoint by inhibiting the Cdc20–APC complex (Dobles et al., 2000; Fang et al., 1998; Li and Benezra, 1996; Li et al., 1997). Tpr has been shown to directly interact with Mad1 and Mad2 proteins through its amino- and carboxy-terminal regions, respectively (Lee et al., 2008). We have previously shown that phosphorylation of Tpr by ERK2 enhances its interaction with ERK2 (Vomastek et al., 2008). Therefore, we wanted to determine whether the ERK-independent phosphorylation events play any role in regulating the interaction between Tpr and the Mad proteins. To this end, FLAG–Tpr-Si and the phosphorylation-site mutants Tpr-Si-S2059A or Tpr-Si-S2094A were co-transfected with either HA–Mad1 or HA–Mad2. The cells lysates were immunoprecipitated with anti-FLAG antibodies and probed for co-immunoprecipitated HA–Mad1 or HA–Mad2. Although the interaction of HA–Mad1 with Tpr and Tpr-Si-S2059A was apparent, we could not detect interaction of HA–Mad1 with Tpr-Si-S2059A (Fig. 7A). By contrast, the interaction of HA–Mad2 with Tpr seems to be independent of phosphorylation on S2059 or S2094 residues (Fig. 7B). Thus, our data strongly suggest a role for S2059 phosphorylation in mediating the Tpr–Mad1 interaction, although a direct effect of the mutation independent of phosphorylation cannot be strictly excluded.

Tpr knockdown has been shown to affect the localization of Mad1 protein and also to result in decreased nuclear accumulation of Mad2 (Lee et al., 2008; supplementary material Fig. S3B). We investigated whether Tpr phosphorylation plays any role in the localization of Mad1 and Mad2 proteins. To this end, HeLa cells

Journal of Cell Science (2014) 127, 3505–3520 doi:10.1242/jcs.149112

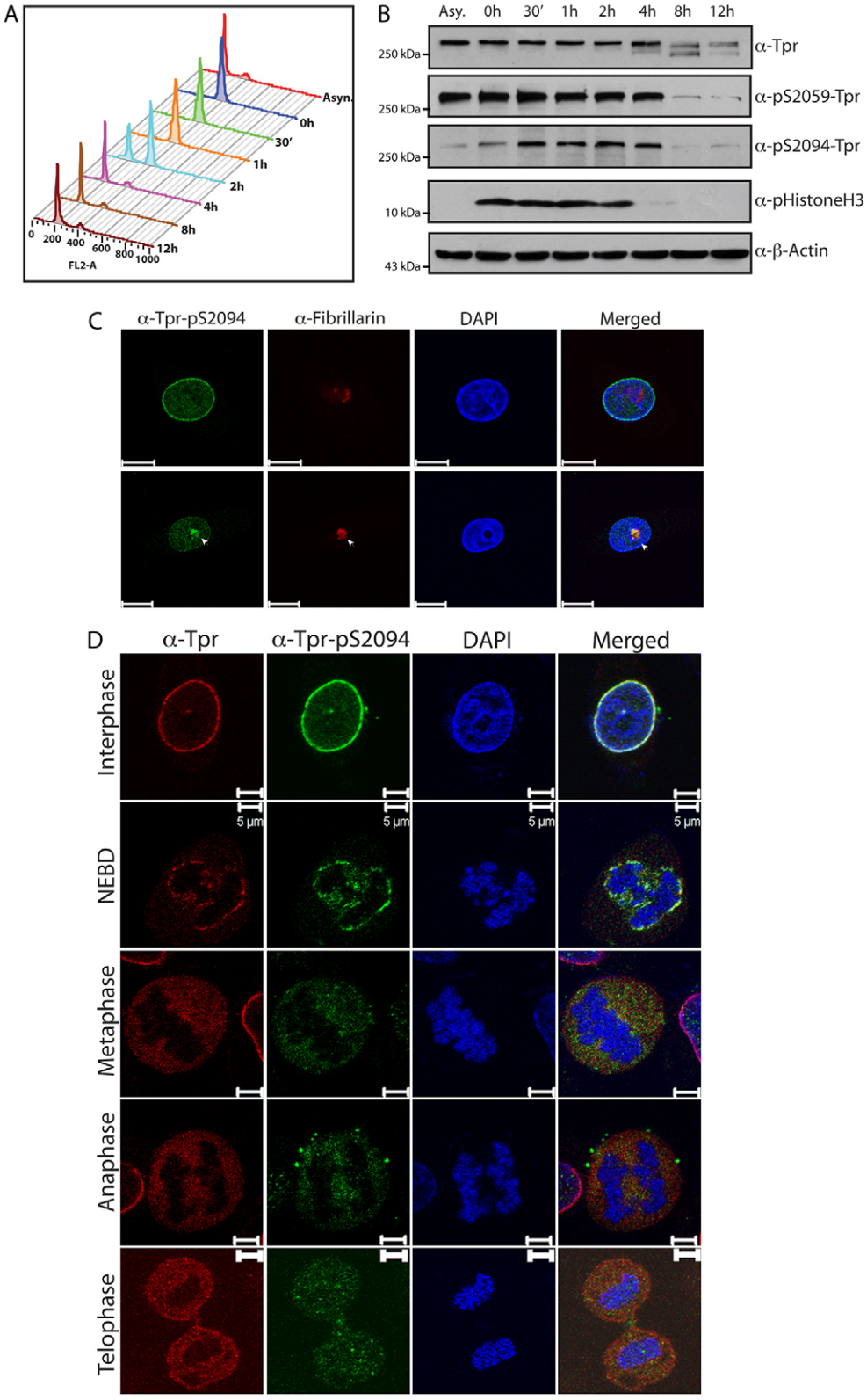

Fig. 5. Localization of S2094-phosphorylated Tpr during cell cycle. (A) HeLa cells were arrested at a pre-mitotic stage by treatment with 40 ng/ml nocodazole and were subsequently released by washing off the drug. Samples were stained with propidium iodide and analyzed by flow cytometry to check for the synchronization of cells after release from the nocodazole block. (B) Western blot analysis of the lysates obtained from cells harvested at different time-points after release from the nocodazole block and probed with anti-Tpr, anti-β-actin, anti-phosphorylated-histone3, anti-Tpr-pS2059 and anti-Tpr-pS2094 antibodies. (C) Immunofluorescence analysis of HeLa cells stained with anti-Tpr-pS2094 (green) and anti-fibrillarin (red) antibodies. Arrowheads indicate the nucleolar staining. Scale bars: 10 μm. (D) Immunofluorescence analysis of an asynchronous HeLa cell population stained with DAPI (DNA, blue) and anti-Tpr (red) and anti-Tpr-pS2094 (green) antibodies. Images of the cells captured at different stages of mitosis are shown. NEBD, nuclear envelope breakdown. Scale bars: 5 μm.

were transfected with Tpr-specific siRNA along with GFP-tagged siRNA-resistant wild-type Tpr (GFP–Tpr-Si) or phosphorylation-site mutants (GFP–Tpr-Si-S2059A and GFP–Tpr-Si-S2094A), and the localization of Mad1 and Mad2 proteins was analyzed by immunofluorescence. In agreement with the previously published data, we clearly observed compromised nuclear-rim staining of Mad1 protein (data not shown) and reduced Mad2 in the nucleus upon Tpr depletion (supplementary material Fig. S3B). The restoration of rim staining of Mad1 was clearly observed upon rescue with GFP–Tpr-Si or GFP–Tpr-Si-S2094A proteins

Journal of Cell Science (2014) 127, 3505–3520 doi:10.1242/jcs.149112

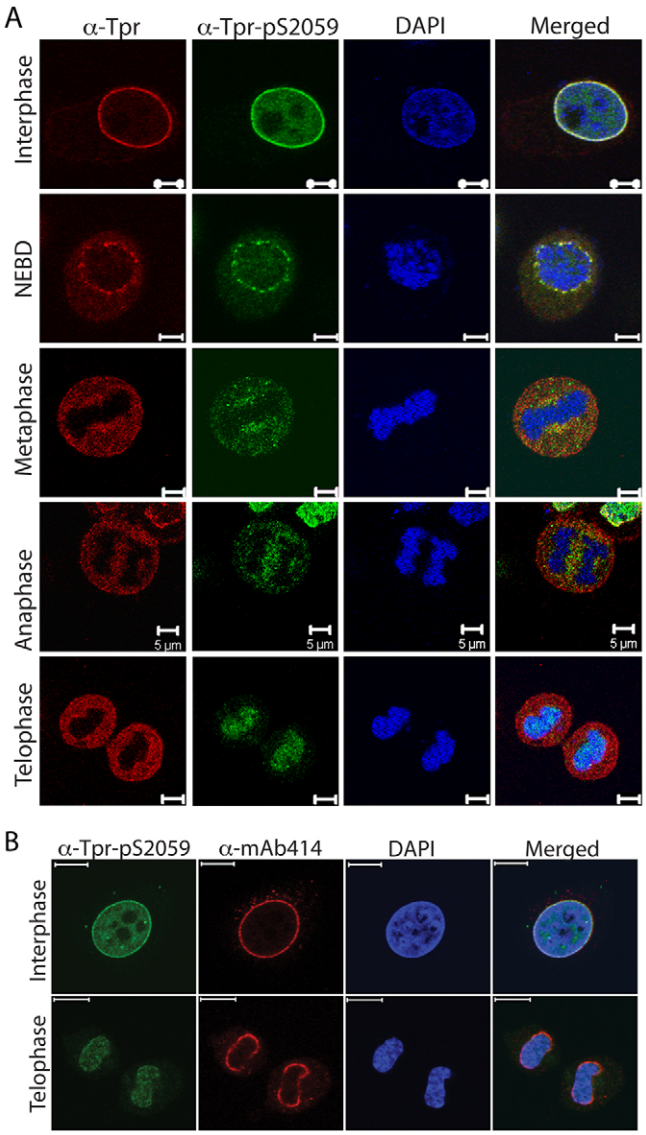

Fig. 6. S2059-phosphorylated Tpr localizes to chromatin at the end of mitosis. (A) Immunofluorescence analysis of an asynchronous HeLa cell population stained with DAPI (DNA, blue) and anti-Tpr-pS2059 (green) and anti-Tpr (red) antibodies. Images of the cells at different mitotic stages are shown. NEBD, nuclear envelope breakdown. Scale bars: 5 μm. (B) Asynchronous HeLa cells were stained with anti-Tpr-pS2059 (green) and mAB414 (red) antibodies. Cells imaged at interphase and telophase are shown. Scale bars: 10 μm.

(Fig. 7C). Interestingly, upon rescue with the phosphorylation-deficient mutant GFP–Tpr-Si-S2059A, we observed diminished nuclear-rim staining of Mad1 protein (Fig. 7C). Similarly, the nuclear localization of Mad2 could be restored upon co-transfection with either GFP–Tpr-Si or GFP–Tpr-Si-S2094A but not with the GFP–Tpr-Si-S2059A mutant (Fig. 7D, GFP-positive cells indicated by arrow). These results clearly demonstrate that phosphorylation at S2059 residue is crucial for Tpr-mediated nuclear localization of the Mad proteins.

Phosphorylation of Tpr is crucial for mediating its role in mitosis

Recently, Tpr-depleted cells were shown to undergo accelerated mitosis, and Tpr-mediated stabilization of Mad1 and Mad2 was shown to be required for a normal spindle assembly checkpoint response (Schweizer et al., 2013). As the data presented in Fig. 7 demonstrated the importance of S2059 phosphorylation for the appropriate localization of Mad proteins, we sought to determine the role of S2059 phosphorylation in mitotic timing. To address this question, Tpr-depleted HeLa cells were rescued with either GFP–Tpr-Si or GFP–Tpr-Si-S2059A constructs. We imaged transiently transfected GFP-positive live cells through mitosis, from the appearance of the metaphase plate until the end of anaphase. In accordance with the findings of Schweizer et al. (Schweizer et al., 2013), the transition time from metaphase to anaphase was shortened in Tpr-depleted cells (Fig. 8A,B). Upon rescue with GFP–Tpr-Si, the mitotic timing was partially restored, whereas the transfection of GFP–Tpr-Si-S2059A failed to rescue the phenotype (the mitotic timing observed was similar to that of Tpr-depleted cells; Fig. 8B). These results imply that phosphorylation of S2059 is crucial for facilitating the role of Tpr in mitosis. Although these results are fascinating, more-detailed investigations with stable cell lines expressing GFP–Tpr-Si and GFP–Tpr-Si-S2059A would help to determine the impact of S2059 phosphorylation on the Tpr–Mad1–Mad2 complex during mitosis.

Depletion of Tpr has been shown to lead to a chromosome-lagging phenotype and results in cell cycle defects such as multinucleation and the presence of micronuclei (Lee et al., 2008). In concurrence with these results, when HeLa cells were depleted of Tpr for ~96 h (by performing two rounds of transfection), we observed micronuclei formation in ~38% cells (Fig. 8C,D). Next, we performed rescue experiments wherein Tpr expression was restored by co-transfecting Tpr-siRNA along with siRNA-resistant GFP–Tpr wild-type or phospho-mutant constructs. The GFP-positive cells (n=50) were then visualized for the presence of micronuclei by confocal microscopy. In the cells transfected with the GFP–Tpr-Si wild-type construct, the occurrence of aberrant micronuclei was reduced to ~9%, suggesting that Tpr function was reinstated upon rescue. However, when we restored Tpr expression using siRNA-resistant GFP–Tpr-Si-S2059A or GFP–Tpr-Si-S2094A, micronuclei were still detected in ~45% of the cell population (Fig. 8E,F). These results indicate that phosphorylation of Tpr on the S2059 and S2094 residues is crucial for the role of Tpr in mitosis.

DISCUSSION

In the present study, we have identified novel *in vivo* phosphorylation sites at S2059 and S2094 in the Tpr protein. We demonstrate that PKA and CDK1 phosphorylate the Tpr protein at S2094 and S2059 residues, respectively. Phosphospecific antibodies were raised against these residues, and these antibodies were found to be specific to the phosphorylated form of the protein. Results indicate that both total Tpr protein levels and its PKA-dependent phosphorylation are regulated during the cell cycle. Specifically, we demonstrate that the S2059-phosphorylated form of the Tpr protein differentially localizes with the chromatin during telophase and that phosphorylation at this residue is crucial for the interaction of Tpr with Mad1 protein. Abrogation of S2059 phosphorylation on Tpr compromises the localization of Mad proteins and results in cell cycle defects.

The mammalian PKA and PKC, the *Saccharomyces cerevisiae* casein kinase and the *Aspergillus nidulans* Ser/Thr kinase NIMA have been shown to phosphorylate NPC components (Cai et al., 2002; De Souza et al., 2004; Lusk et al., 2007; Miller et al.,

Journal of Cell Science (2014) 127, 3505–3520 doi:10.1242/jcs.149112

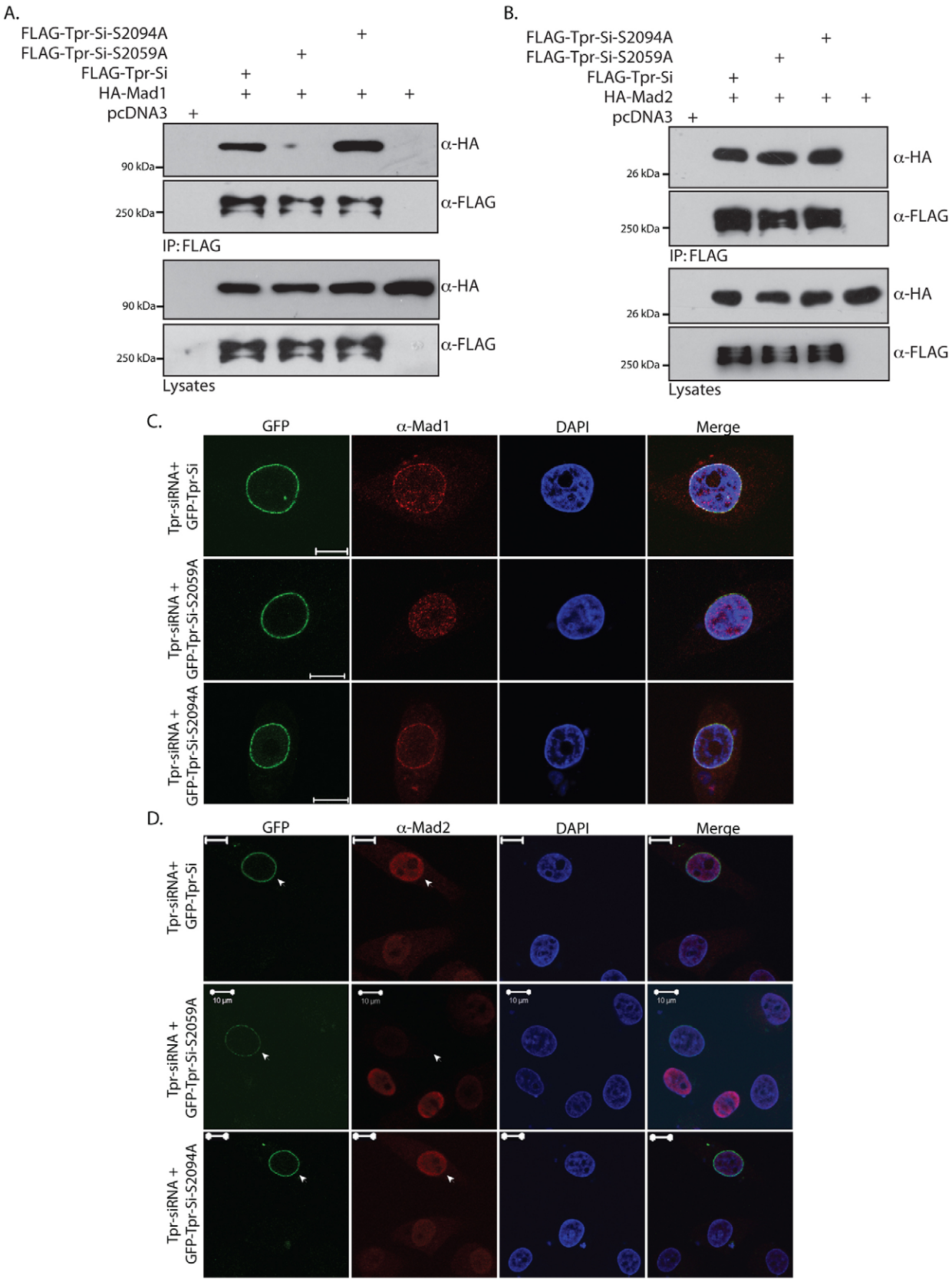

Fig. 7. See next page for legend.

Fig. 7. Phosphorylation at S2059 is required for the interaction of Tpr with Mad1 and the correct localization of Mad proteins. (A) COS-1 cells were transfected with pCDNA3-FLAG construct or constructs encoding FLAG–Tpr-Si, FLAG–Tpr-Si-S2059A, FLAG–Tpr-Si-S2094A or HA–Mad1. At 36 h post-transfection, cells were lysed, and the lysates were immunoprecipitated (IP) with anti-FLAG antibodies. The immunoblots were probed with anti-FLAG and anti-HA antibodies to check for the presence of the interacting HA–Mad1 protein. (B) COS-1 cells were transfected with pCDNA3-FLAG construct or constructs encoding FLAG–Tpr-Si, FLAG–Tpr-Si-S2059A, FLAG–Tpr-Si-S2094A or HA–Mad2. At 36 h post-transfection, the lysates were immunoprecipitated with anti-FLAG antibodies. Western blot analysis was performed using anti-FLAG and anti-HA antibodies to check for the presence of interacting Mad2 protein. (C) HeLa cells were co-transfected with Tpr-specific siRNA along with GFP–Tpr-Si or GFP–Tpr-Si-S2059A or GFP–Tpr-Si-S2094A constructs. The next day, the cells were replated and, 24 h later, the cells were re-transfected with Tpr-specific siRNA and the same constructs. At 96 h after the first transfection, cells were stained with anti-Mad1 antibodies (red) and analyzed by confocal microscopy. Scale bars: 10 μm. (D) HeLa cells were co-transfected with Tpr-specific siRNA along with GFP–Tpr-Si, GFP–Tpr-Si-S2059A or GFP–Tpr-Si-S2094A constructs. At 48 h post-transfection, cells were stained with anti-Mad2 antibodies (red) and analyzed by confocal microscopy. Arrowheads indicate cells transfected with GFP constructs. Scale bars: 10 μm.

1999). Phosphorylation of structural proteins of the NPC by PKA or PKC has been suggested to be necessary for nuclear import (Karin and Hunter, 1995; Nigg, 1990; Nigg, 1997; Pemberton and Paschal, 2005; Terry et al., 2007; Wen et al., 1995). We have previously shown that although Tpr has a limited role in protein transport through the NPC, it specifically regulates the export of CTE-dependent unspliced RNAs (Rajanala and Nandicoori, 2012). The results from our study suggest that phosphorylation of Tpr by PKA does not have any impact on the known transport function of Tpr. In our study, we observed that S2094-phosphorylated Tpr localizes to the nucleolar compartment. The nucleolar compartment serves as a major hub for ribosome biogenesis, ribosomal (r)RNA processing and transcription (Aitchison and Rout, 2000; Lewis and Tollervey, 2000). Several studies have reported that important factors which regulate cell division, senescence, pre-mRNA processing, mRNA export, stress response and telomere activity are transiently localized to the nucleolus (Boisvert et al., 2007; Boulon et al., 2010; Johnson et al., 1998; Olson et al., 2000; Pederson, 1998; Raška et al., 2006). The stage-specific nucleolar sequestration of certain cell cycle proteins, such as Cdc14 and Mdm2, has been shown to regulate their activity and to be crucial for cell cycle progression, by preventing early mitotic exit (Shou et al., 1999; Tao and Levine, 1999; Visintin and Amon, 2000; Visintin et al., 1999; Weber et al., 1999). Further detailed analysis needs to be performed to examine the functional significance of nucleolar sequestration of S2094-phosphorylated Tpr.

Mitotic kinases, such as Aurora kinase, PLK, Nek (NIMA-related kinase) and CDK1, phosphorylate several nucleoporins and the members of the spindle assembly and thereby have been shown regulate crucial mitotic check points (Barr et al., 2004; Ducat and Zheng, 2004; Fry et al., 2012; Ma and Poon, 2011; Petronczki et al., 2008; Portier et al., 2007). In our study, we observed that CDK1 phosphorylates Tpr on the S2059 residue. The PLK1-dependent phosphoproteomic analysis of the human mitotic spindle specifically demonstrated that many proteins of the spindle assembly, including Mad1 and several nucleoporins, such as Nup98, Nup153 and Tpr, were substrates for PLK1 (Santamaria et al., 2011). The site for the PLK1 phosphorylation on the Tpr protein has been found to be the S1185 residue (Santamaria et al., 2011). In addition, in our study, we identify the S2034 residue on the C-terminal region of Tpr as a consensus site for PLK1 phosphorylation. Depletion of PLK1 has been found to decrease the association of Mad1 and Mad2 proteins to the kinetochore (Ahonen et al., 2005; Kang et al., 2006). It was speculated that the phosphorylation of proteins by PLK1 might influence their localization to the spindles (Santamaria et al., 2011). However, PLK1 was not found to be crucial for the progression of mitosis controlled by the spindle checkpoint (Petronczki et al., 2008).

Studies by various groups have tried to decipher the factors involved along with Mad1 and Mad2 proteins in regulating the spindle assembly checkpoint during mitosis. In budding yeast, it has been demonstrated that phosphorylation of Bub1 by Mps1 is essential for the Mps1-mediated recruitment of Mad1–Mad2 complexes to the kinetochores (London and Biggins, 2014). The interaction of Mad1 protein with Bub1 has been found to be crucial for the targeting of Mad1–Mad2 complexes to the kinetochores (Heinrich et al., 2014; Moyle et al., 2014). The phosphorylation of Mad1 by ATM kinase was shown to be crucial for its heterodimerization with Mad2 (Yang et al., 2014). Apart from the kinetochore recruitment of Mad2, Mad1 has additional functions in regulating SAC (Heinrich et al., 2014; Kruse et al., 2014). Furthermore, it is known that the timely relocalization of Mad1 to kinetochores during metaphase can restore initially silenced SAC activity (Kuijt et al., 2014). The nucleoporin Tpr has been shown to be crucial for the maintenance of SAC proteostasis in all stages of the cell cycle. Tpr is essential for the localization of Mad2 but not Mad1 to the kinetochores (Schweizer et al., 2013).

Previously, Tpr has been shown to directly interact with Mad1 and Mad2 proteins through its N-terminus and C-terminus, respectively (Lee et al., 2008, Nakano et al., 2010). Co-immunoprecipitation experiments revealed that although the interaction of Tpr with Mad1 is modulated by S2059 phosphorylation, its interaction with Mad2 seems to be independent of Tpr phosphorylation. Using immunofluorescence experiments, we found that the localization of both Mad1 and Mad2 proteins was dependent on the S2059 phosphorylation of Tpr. This was somewhat unexpected in light of the data from the co-immunoprecipitation experiments. Lee et al. have suggested (Lee et al., 2008) that Tpr might act in a manner akin to a scaffold at the pore, thus being required for the localization of Mad1 and Mad2 proteins to the pore. It is possible that the abrogation of phosphorylation on the S2059 residue of Tpr affects its suggested functional role as a scaffolding protein at the NPC, thus having an impact on the localization of both Mad proteins.

Cdk1-mediated phosphorylation has been shown to regulate the breakdown of the nuclear envelope at mitosis and the dissociation of the NPC into different subcomplexes (Lusk et al., 2007; Macaulay et al., 1995; Mühlhäusser and Kutay, 2007; Onischenko et al., 2005). The phosphorylation of Nup98 has been shown to be essential for NPC dissociation (Laurell et al., 2011). After mitosis, the NPC is reassembled at the pore step-wise, and Tpr has been shown to be recruited at the last stage (Bodoor et al., 1999; Hase and Codes, 2003). In agreement with this data, we observed that whereas both FG-Nups and Nup153 began associating with the nuclear membrane during telophase, both Tpr and S2059-phosphorylated Tpr have not yet been recruited to NPC. An independent study has shown that the nucleoporin Tpr is important for establishing nucleopore-associated HEZs and thereby mediating the formation of distinct intranuclear subcompartments (Krull et al., 2010). The

Journal of Cell Science (2014) 127, 3505–3520 doi:10.1242/jcs.149112

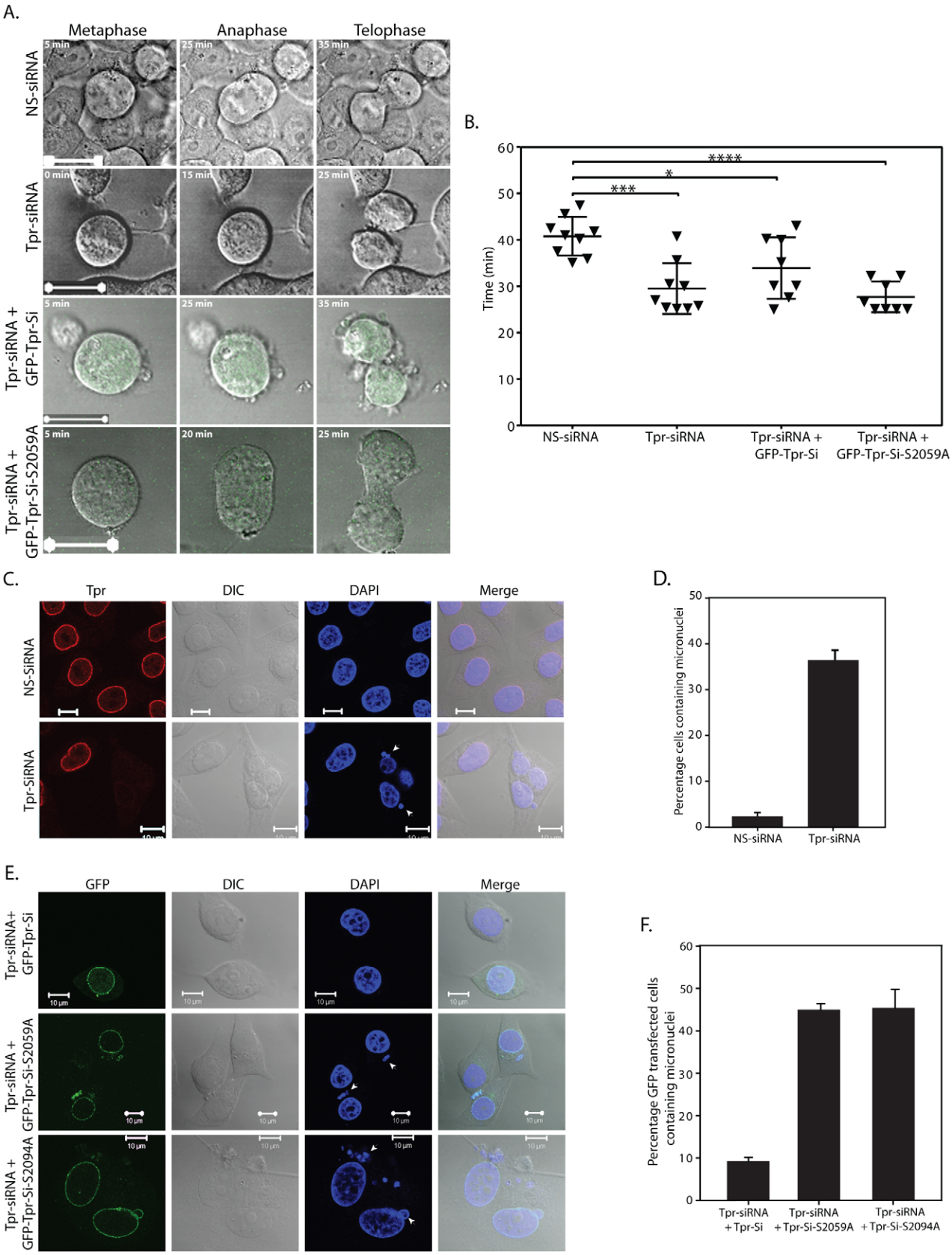

Fig. 8. See next page for legend.

Fig. 8. Tpr-depleted cells rescued with phospho-mutants display cell cycle defects. (A) Live-cell analysis of HeLa cells transfected with NS-siRNA or Tpr-specific siRNA, and cells that were rescued with either GFP–Tpr-Si or GFP–Tpr-Si-S2059A constructs. Representative images of cells at metaphase, anaphase and telophase are shown. Scale bars: 20 µm. (B) Analysis of the mitotic timing measured from metaphase until the end of anaphase. Data was obtained from two independent experiments in which cells were treated with control siRNA (40±4.15 min; $n=9$), depleted of Tpr (29.5±5.45 min; $n=9$) or depleted of Tpr followed by rescue with either GFP–Tpr-Si (33.91±6.6 min; $n=8$) or GFP–Tpr-Si-S2059A (27.72±3.29 min; $n=8$). Data show the mean±s.d.; $^{*}P=0.0413$; $^{***}P=0.0003$; $^{****}P<0.0001$. (C) HeLa cells transfected with NS-siRNA or Tpr-specific siRNA were replated the next day and, 24 h later, the cells were again transfected with the same siRNA oligos. After ~96 h of Tpr depletion, the cells were stained with anti-Tpr antibodies (red) to visualize the presence of nuclear defects resulting from Tpr knockdown. DIC, differential interference contrast. (D) Quantification of the percentage of HeLa cells ($n=50$) containing micronuclei after ~96 hours of Tpr depletion. Data show the mean±s.d. (two independent experiments). (E) HeLa cells were transfected with Tpr-specific siRNA along with constructs encoding GFP–Tpr-Si, GFP–Tpr-Si-S2059A or GFP–Tpr-Si-S2094A. Immunofluorescence analysis was performed at ~96 h after the first transfection. Arrowheads indicate the presence of micronuclei. Scale bars: 10 µm. (F) Quantification of the percentage of HeLa cells containing micronuclei after ~96 h of Tpr depletion and following rescue with GFP–Tpr-Si, GFP–Tpr-Si-S2059A or GFP–Tpr-Si-S2094A. Data show the mean±s.d. ($n=50$, two independent experiments).

results obtained in this study specifically indicate that Tpr phosphorylated at the S2059 residue associates with the chromatin at the telophase, just before the NPC reassembly. The association of S2059-phosphorylated Tpr with chromatin during telophase might also influence the ability of Tpr ability to mediate nucleopore-associated perinuclear HEZs during the re-formation of nuclear envelope.

The observations presented in this study unequivocally demonstrate the importance of phosphorylation of Tpr on S2059 and the S2094 residues in mitotic progression. Previous reports have established the fact that Tpr acts as a scaffold that recruits proteins that are required for chromosome segregation, such as the Mad proteins and members of the dynein complex (Lee et al., 2008). The necessity of S2059 phosphorylation for Tpr–Mad1 interaction and localization suggests that S2059 phosphorylation might modulate the scaffolding function of Tpr. Although S2094 phosphorylation does not seem to have any effect on the Tpr–Mad1 interaction or Mad2 subcellular localization, the inability of the mutant to rescue the chromosome-lagging phenotype suggests a crucial role for S2094 phosphorylation. An in-depth study of the mechanistic details of Tpr phosphorylation would assist us in investigating how crucial functions, such as spindle assembly and chromatin organization, are modulated by Tpr, throwing more light on how various cellular processes are regulated by the NPC during the different stages of the cell cycle.

MATERIALS AND METHODS

Plasmid constructs, antibodies, inhibitors and siRNA

The construction of pcDNA3-Tpr, pcDNA3-TprC (TprC) and TprC-M4 and Tpr-M4-Si have been reported previously (Vomastek et al., 2008). The pcDNA-TprC-M4-(S2059A), TprC-S2059A, TprC-M4-(S2094A) and TprC-S2094A constructs were made by overlapping PCR using appropriate mutagenic primers, and the mutations were confirmed by DNA sequencing. The full-length clones FLAG–Tpr-Si-S2059A and FLAG–Tpr-Si-S2094A were made by subcloning the *Not*I–*Ppu*MI fragments from TprC-S2059A and TprC-S2094A constructs into the corresponding sites in the plasmid encoding FLAG–Tpr-Si (Vomastek et al. 2008). The CMV-PKA plasmid was kindly provided by Pushkar Sharma (National Institute of Immunology, New Delhi, India). The plasmids encoding GFP–Tpr-Si, GFP–Tpr-Si-S2059A and GFP–Tpr-Si-S2094A were generated by amplifying the ~7.5-kb full-length Tpr gene from corresponding constructs encoding FLAG–Tpr using Phusion DNA polymerase (New England Biolabs) and cloning the amplicons into pcDNA6.2/C-EmGFP (Invitrogen).

The anti-Tpr mouse monoclonal antibody (ab58344) and antibodies against nuclear pore complex proteins (mAb414), fibrillarin, Mad1, Mad2 and β-actin were obtained from Abcam. The rabbit polyclonal anti-Tpr antibody was kindly provided by Larry Gerace (Frosst et al., 2002). The antibodies against ERK2, pS133-CREB, PKA, HA and phosphorylated histone 3 were purchased from Cell Signaling Technology. The anti-Nup153 antibody was obtained from Santa Cruz Biotechnology. The anti-FLAG antibodies were obtained from Sigma. The phosphospecific antibodies used in this study were custom-made by PhosphoSolutions (Aurora, CO). The CREST anti-sera was kindly provided by Mary Dasso (NIH, Bethesda, MD). All the secondary antibodies were obtained from Jackson Immuno Research Laboratories. NS-siRNA, Tpr-specific siRNA (Rajanala and Nandicoori 2012) and the PKA-specific siRNA were obtained from Dharmacon. The inhibitors used were against GSK3β (Inhibitor VIII, Calbiochem), PLK (BI2536, Sigma), p38 kinase (SB203580, Sigma), Aurora kinase (MLN8237, Shelleck) (gifted by Tapas Kundu, Indian Institute of Science, New Delhi, India) and CDK1 (RO3306, Calbiochem) (gifted by Sandeep Saxena, National Institute of Immunology, New Delhi, India).

p24 ELISA and β-galactosidase assay

The p24 ELISA and β-galactosidase assay were performed in HEK-293T cells as described previously (Rajanala and Nandicoori, 2012). Briefly, HEK-293T cells were transfected with 1 µg of NS-siRNA or Tpr-specific siRNA along with 2 µg of construct encoding FLAG–Tpr-Si, FLAG–Tpr-Si-S2059A or FLAG–Tpr-Si-S2094A, 250 ng of pCMV-Gag/Pol-CTE and 100 ng of pCMV-β-Gal reporter constructs. At 48 h post-transfection, the cells were replated and re-transfected. At 96 h post-transfection, cells were lysed and the p24 levels and β-galactosidase activity in the lysates were determined as described previously (Rajanala and Nandicoori, 2012).

Cell culture and transfection

COS-1 cells and HeLa cells were grown in DMEM supplemented with 10% fetal bovine serum (FBS). All transfections were performed using Lipofectamine 2000 reagent (Invitrogen) according to the manufacturer's instructions. For observing the micronuclei upon Tpr depletion, HeLa cells transfected with NS-siRNA or Tpr-specific siRNA were replated the next day and, 24 h later, the cells were again transfected with the siRNAs and incubated for an additional 48 h. At ~96 h after the original transfection, the samples were analyzed by immunofluorescence.

Immunofluorescence

The cells were plated on coverslips and fixed in 4% paraformaldehyde. The cells were then permeabilized using 0.1% Triton X-100 and blocked with 10% chicken serum. The coverslips were mounted in Vectashield anti-fade medium containing DAPI (Vecta Laboratories), and images were acquired with the help of Carl Zeiss Axiovision LSM 510 Meta confocal microscope using LSM5 software.

Metabolic labeling, phosphopeptide mapping and phospho-amino-acid analysis

COS-1 cells grown in 100-mm dishes were transfected with 8 µg of constructs, and the cells were metabolically labeled for 3 h and stimulated with EGF (20 ng/ml) for 10 min. The metabolic labeling of COS-1 cells, as well as phosphopeptide mapping and phospho-amino-acid analysis, were performed as described previously (Vomastek et al., 2008).

Purification of the C-terminal fragment of Tpr from *E. coli*

Plasmids pQE2-TprC, TprC-S2059A or TprC-S2094A expressing the carboxy-terminal fragments of Tpr were transformed into *E. coli* BL21

(DE3) Codon Plus cells (Stratagene). Cultures in the exponential phase of growth were induced with 0.1 mM IPTG and incubated for 3 h at 37℃. Cells were harvested, lysed by sonication in lysis buffer (20 mM Tris-HCl pH 7.5, 200 mM NaCl and 10 mM β-mercaptoethanol) and clarified by high-speed centrifugation. The cell lysates containing His-fusion recombinant protein were nutated with equilibrated Ni–NTA agarose (GE Healthcare) affinity resin. His-tagged protein was eluted with lysis buffer containing 50–200 mM imidazole. Peak fractions were pooled and dialysed against storage buffer (10 mM Tris-HCl pH 7.4, 50 mM NaCl and 20% glycerol).

In vitro kinase assay

COS-1 cells were transfected with 8 µg each of constructs encoding wild-type FLAG–TprC, FLAG–TprC-S2059A, FLAG–TprC-S2094A, HA–ERK2 and CMV-PKA. The lysates of cells obtained at 36 h post-transfection were immunoprecipitated with anti-FLAG, anti-HA or anti-PKA antibodies. The immunoprecipitated FLAG–TprC was mixed with immunoprecipitated HA–ERK2 and the kinase reaction was performed in kinase buffer (25 mM HEPES pH 7.4, 20 mM magnesium acetate and 1 mM dithiothreitol) containing 10 µCi [γ-^{32}P]-ATP (Perkin Elmer, Boston, MA), at 30℃ for 10 min. The immunoprecipitated CMV-PKA sample was distributed and mixed either with the immunoprecipitated FLAG–TprC, FLAG–TprC-S2059A or FLAG–TprC-S2094A samples, and kinase reactions were carried out for 10 min at 30℃. The reactions were stopped by adding 2× SDS sample buffer, followed by heating at 95℃ for 5 min. The samples were resolved by SDS-PAGE followed by transfer onto nitrocellulose membrane and autoradiography.

To carry out the kinase assays with CDK1, the CDK1–cyclinB active complex was purchased from New England Biolabs. A total of 5 µg of MBP or 1 µg of purified wild-type or mutant His-TprC fragments were incubated with 20 U of CDK1–cyclinB complex, and the kinase reactions were performed with 10 µCi [γ-^{32}P]-ATP in the buffer provided by manufacturer.

Characterization of phospho-specific antibodies

COS-1 cells were transfected with 2 µg each of pCDNA3-FLAG, FLAG-TprC, FLAG-TprC-S2059A or FLAG-TprC-S2094A constructs. The lysates obtained at 36 h after transfection were loaded alongside the purified bacterial TprC protein. The samples were resolved, transferred onto nitrocellulose membrane and the blot was probed with antibodies against FLAG, ERK, Tpr, S2059-phosphorylated Tpr and S2094-phosphorylated Tpr. For the detection of full-length Tpr protein, COS-1 cells in six-well plates were transfected with 2 µg each of pCDNA3-FLAG, FLAG-Tpr-Si, FLAG–Tpr-Si-S2059A or FLAG–Tpr-Si-S2094A constructs. The lysates were then analyzed with antibodies against FLAG, ERK, S2059-phosphorylated Tpr and pS2059-phosphorylated Tpr.

Cell cycle synchronization and flow cytometry analysis

HeLa cells were grown in dishes of 100-mm diameter and treated with nocodazole (40 ng/ml) for 16 h. The mitotic cells were shaken off, and the released cells were replated in drug-free medium. The cells harvested at different time-points after nocodazole release were fixed in 70% ethanol at 4℃ with constant agitation for 16–18 h. Cells were washed three times with 1× PBS and resuspended in appropriate amounts of propidium iodide/RNase staining solution (BD Biosciences). After incubation for 15 min, the cells were analyzed by flow cytometry (BD FACS Calibur) using Cell Quest Software (BD Biosciences).

Immunoprecipitation

COS-1 cells plated on 100-mm dishes were transfected with different plasmid constructs (individually or in combination) using Lipofectamine 2000 (Invitrogen). Cells were harvested 36 h after transfection. To detect co-immunoprecipitated HA–Mad1, cells were lysed with M2 lysis buffer (50 mM Tris-HCl, 150 mM NaCl, 10% glycerol, 1% Triton X-100, 0.5 mM EGTA and 0.5 mM EDTA) containing protease inhibitor cocktail (Roche). To detect co-immunoprecipitated Mad2, hypotonic lysis buffer (20 mM HEPES pH 7.4, 2 mM EGTA, 2 mM $MgCl_2$, 200 mM sodium orthovanadate and protease inhibitor cocktail) was used for cell lysis. The lysates were clarified by high-speed centrifugation and the FLAG-tagged Tpr was immunoprecipitated with the help of anti-FLAG-M2–agarose beads (Sigma). Immunoprecipitates were resolved by SDS-PAGE on a 10% gel, followed by western blot analysis with different antibodies.

Identification of phosphorylation sites by mass spectrometry

COS-1 cells on 100-mm dishes were transfected with FLAG–TprC-M4, the cells were harvested at 24 h post-transfection and FLAG-tagged TprC-M4 was immunoprecipitated as described above. FLAG–TprC-M4 bound to the beads was eluted using 0.2 M glycine (pH 2.0) and the eluate was immediately neutralized by the addition of 1 M Tris-HCl (pH 8.0). The eluate was dried and resuspended in freshly prepared digestion buffer (8 M urea in 25 mM NH_4HCO_3), followed by reduction and alkylation (Jagtap et al., 2012). Samples were diluted with 25 mM NH_4HCO_3 to a final concentration of 1 M urea and processed and analyzed as described previously, except that spectra were queried against the *Homo sapiens* UniProt database (Jagtap et al., 2012). Precursor Ions Area Detector node of proteome discoverer 1.3 (Thermo) was used to calculate the area of all the identified peptides. The stoichiometry of phosphorylation was determined using the equation [(area of phosphorylated peptide/area of phosphorylated peptide+area of non-phosphorylated peptide)×100].

2D gel electrophoresis

COS-1 cells in 100-mm dishes were transfected with FLAG–TprC-M4, FLAG–TprC-M4-S2059A or FLAG–TprC-M4-S2094A and, 24 h post-transfection, FLAG-tagged proteins were immunoprecipitated. Bound proteins were eluted using 2× SDS sample buffer, and eluted proteins were precipitated with five volumes of cold acetone. Precipitated proteins were resuspended in 300 µl of 2D sample buffer and resolved on pH 3.5–5.6 IPG strips (GE) as described previously, followed by western blotting using anti-FLAG antibodies (Khan et al., 2010).

Live-cell imaging and statistical analysis

Transfected HeLa cells grown in DMEM supplemented with 10% FBS at 37℃ under 5% CO_2 were imaged over time in a dedicated live-cell chamber attached to a Carl Zeiss Axiovision LSM 510 Meta confocal system using the 63× oil-immersion objective. The acquired time-lapse images were analyzed using the LSM5 software. Statistical analysis was performed using Graphpad Prism version 6.04. One way ANOVA analysis was performed to analyze differences between the means of the groups under study.

Acknowledgements

We thank all our colleagues who have provided the reagents used in this study. We thank the Central Confocal Microscopy, Flow Cytometry and Mass spectrometry facilities at the National Institute of Immunology (NII). We thank Vijay Soni (NII, New Delhi, India) for the cloning of His-TprC, His-TprC-S2059A and His-TprC-S2094A. We acknowledge Shanta Sen (NII, New Delhi, India) for her support in managing the mass spectrometry facility. We thank Gargi Roy, Sangeeta Kumari and Amrita Ramkumar (all of the NII, New Delhi, India) for their assistance in the project.

Competing interests

The authors declare no competing interests.

Author contributions

K.R. and V.K.N. conceived and designed the experiments. K.R., A.S., G.D.J., R.P. and M.J. performed the experiments. K.R., S.S., G.D.J. and V.K.N. analyzed the data. K.R. and V.K.N. wrote the paper.

Funding

This work was supported by funding provided by the Department of Biotechnology (DBT), Government of India [grant number BT/PR 11056/BRB/10/632/2008] to V.K.N. G.D.J. is a Wellcome-Department of Biotechnology Early Career Fellow. Deposited in PMC for release after 6 months.

Supplementary material

Supplementary material available online at
http://jcs.biologists.org/lookup/suppl/doi:10.1242/jcs.149112/-/DC1

References

Ahonen, L. J., Kallio, M. J., Daum, J. R., Bolton, M., Manke, I. A., Yaffe, M. B., Stukenberg, P. T. and Gorbsky, G. J. (2005). Polo-like kinase 1 creates the tension-sensing 3F3/2 phosphoepitope and modulates the association of spindle-checkpoint proteins at kinetochores. *Curr. Biol.* **15**, 1078-1089.

Aitchison, J. D. and Rout, M. P. (2000). The road to ribosomes. Filling potholes in the export pathway. *J. Cell Biol.* **151**, F23-F26.

Barr, F. A., Silljé, H. H. and Nigg, E. A. (2004). Polo-like kinases and the orchestration of cell division. *Nat. Rev. Mol. Cell Biol.* **5**, 429-440.

Blethrow, J. D., Glavy, J. S., Morgan, D. O. and Shokat, K. M. (2008). Covalent capture of kinase-specific phosphopeptides reveals Cdk1-cyclin B substrates. *Proc. Natl. Acad. Sci. USA* **105**, 1442-1447.

Bodoor, K., Shaikh, S., Salina, D., Raharjo, W. H., Bastos, R., Lohka, M. and Burke, B. (1999). Sequential recruitment of NPC proteins to the nuclear periphery at the end of mitosis. *J. Cell Sci.* **112**, 2253-2264.

Boisvert, F. M., van Koningsbruggen, S., Navascués, J. and Lamond, A. I. (2007). The multifunctional nucleolus. *Nat. Rev. Mol. Cell Biol.* **8**, 574-585.

Boulon, S., Westman, B. J., Hutten, S., Boisvert, F. M. and Lamond, A. I. (2010). The nucleolus under stress. *Mol. Cell* **40**, 216-227.

Cai, Y., Gao, Y., Sheng, Q., Miao, S., Cui, X., Wang, L., Zong, S. and Koide, S. S. (2002). Characterization and potential function of a novel testis-specific nucleoporin BS-63. *Mol. Reprod. Dev.* **61**, 126-134.

Clarke, D. J. and Bachant, J. (2008). Kinetochore structure and spindle assembly checkpoint signaling in the budding yeast, Saccharomyces cerevisiae. *Front. Biosci.* **13**, 6787-6819.

Coyle, J. H., Guzik, B. W., Bor, Y. C., Jin, L., Eisner-Smerage, L., Taylor, S. J., Rekosh, D. and Hammarskjöld, M. L. (2003). Sam68 enhances the cytoplasmic utilization of intron-containing RNA and is functionally regulated by the nuclear kinase Sik/BRK. *Mol. Cell. Biol.* **23**, 92-103.

Coyle, J. H., Bor, Y. C., Rekosh, D. and Hammarskjold, M. L. (2011). The Tpr protein regulates export of mRNAs with retained introns that traffic through the Nxf1 pathway. *RNA* **17**, 1344-1356.

David-Watine, B. (2011). Silencing nuclear pore protein Tpr elicits a senescent-like phenotype in cancer cells. *PLoS ONE* **6**, e22423.

De Souza, C. P., Osmani, A. H., Hashmi, S. B. and Osmani, S. A. (2004). Partial nuclear pore complex disassembly during closed mitosis in Aspergillus nidulans. *Curr. Biol.* **14**, 1973-1984.

Dobles, M., Liberal, V., Scott, M. L., Benezra, R. and Sorger, P. K. (2000). Chromosome missegregation and apoptosis in mice lacking the mitotic checkpoint protein Mad2. *Cell* **101**, 635-645.

Ducat, D. and Zheng, Y. (2004). Aurora kinases in spindle assembly and chromosome segregation. *Exp. Cell Res.* **301**, 60-67.

Eblen, S. T., Kumar, N. V., Shah, K., Henderson, M. J., Watts, C. K., Shokat, K. M. and Weber, M. J. (2003). Identification of novel ERK2 substrates through use of an engineered kinase and ATP analogs. *J. Biol. Chem.* **278**, 14926-14935.

Fang, G., Yu, H. and Kirschner, M. W. (1998). The checkpoint protein MAD2 and the mitotic regulator CDC20 form a ternary complex with the anaphase-promoting complex to control anaphase initiation. *Genes Dev.* **12**, 1871-1883.

Favreau, C., Worman, H. J., Wozniak, R. W., Frappier, T. and Courvalin, J. C. (1996). Cell cycle-dependent phosphorylation of nucleoporins and nuclear pore membrane protein Gp210. *Biochemistry* **35**, 8035-8044.

Fontoura, B. M., Dales, S., Blobel, G. and Zhong, H. (2001). The nucleoporin Nup98 associates with the intranuclear filamentous protein network of TPR. *Proc. Natl. Acad. Sci. USA* **98**, 3208-3213.

Frosst, P., Guan, T., Subauste, C., Hahn, K. and Gerace, L. (2002). Tpr is localized within the nuclear basket of the pore complex and has a role in nuclear protein export. *J. Cell Biol.* **156**, 617-630.

Fry, A. M., O'Regan, L., Sabir, S. R. and Bayliss, R. (2012). Cell cycle regulation by the NEK family of protein kinases. *J. Cell Sci.* **125**, 4423-4433.

Funasaka, T., Tsuka, E. and Wong, R. W. (2012). Regulation of autophagy by nucleoporin Tpr. *Sci. Rep.* **2**, 878.

Glavy, J. S., Krutchinsky, A. N., Cristea, I. M., Berke, I. C., Boehmer, T., Blobel, G. and Chait, B. T. (2007). Cell-cycle-dependent phosphorylation of the nuclear pore Nup107-160 subcomplex. *Proc. Natl. Acad. Sci. USA* **104**, 3811-3816.

Harel, A. and Forbes, D. J. (2004). Importin beta: conducting a much larger cellular symphony. *Mol. Cell* **16**, 319-330.

Heinrich, S., Sewart, K., Windecker, H., Langegger, M., Schmidt, N., Hustedt, N. and Hauf, S. (2014). Mad1 contribution to spindle assembly checkpoint signalling goes beyond presenting Mad2 at kinetochores. *EMBO Rep.* **15**, 291-298.

Hetzer, M., Gruss, O. J. and Mattaj, I. W. (2002). The Ran GTPase as a marker of chromosome position in spindle formation and nuclear envelope assembly. *Nat. Cell Biol.* **4**, E177-E184.

Jagtap, P. K., Soni, V., Vithani, N., Jhingan, G. D., Bais, V. S., Nandicoori, V. K. and Prakash, B. (2012). Substrate-bound crystal structures reveal features unique to Mycobacterium tuberculosis N-acetyl-glucosamine 1-phosphate uridyltransferase and a catalytic mechanism for acetyl transfer. *J. Biol. Chem.* **287**, 39524-39537.

Johnson, F. B., Marciniak, R. A. and Guarente, L. (1998). Telomeres, the nucleolus and aging. *Curr. Opin. Cell Biol.* **10**, 332-338.

Kang, Y. H., Park, J. E., Yu, L. R., Soung, N. K., Yun, S. M., Bang, J. K., Seong, Y. S., Yu, H., Garfield, S., Veenstra, T. D. et al. (2006). Self-regulated Plk1 recruitment to kinetochores by the Plk1-PBIP1 interaction is critical for proper chromosome segregation. *Mol. Cell* **24**, 409-422.

Karin, M. and Hunter, T. (1995). Transcriptional control by protein phosphorylation: signal transmission from the cell surface to the nucleus. *Curr. Biol.* **5**, 747-757.

Khan, S., Nagarajan, S. N., Parikh, A., Samantaray, S., Singh, A., Kumar, D., Roy, R. P., Bhatt, A. and Nandicoori, V. K. (2010). Phosphorylation of enoyl-acyl carrier protein reductase InhA impacts mycobacterial growth and survival. *J. Biol. Chem.* **285**, 37860-37871.

Kosako, H. and Imamoto, N. (2010). Phosphorylation of nucleoporins: signal transduction-mediated regulation of their interaction with nuclear transport receptors. *Nucleus* **1**, 309-313.

Kosako, H., Yamaguchi, N., Aranami, C., Ushiyama, M., Kose, S., Imamoto, N., Taniguchi, H., Nishida, E. and Hattori, S. (2009). Phosphoproteomics reveals new ERK MAP kinase targets and links ERK to nucleoporin-mediated nuclear transport. *Nat. Struct. Mol. Biol.* **16**, 1026-1035.

Krull, S., Dörries, J., Boysen, B., Reidenbach, S., Magnius, L., Norder, H., Thyberg, J. and Cordes, V. C. (2010). Protein Tpr is required for establishing nuclear pore-associated zones of heterochromatin exclusion. *EMBO J.* **29**, 1659-1673.

Kruse, T., Larsen, M. S., Sedgwick, G. G., Sigurdsson, J. O., Streicher, W., Olsen, J. V. and Nilsson, J. (2014). A direct role of Mad1 in the spindle assembly checkpoint beyond Mad2 kinetochore recruitment. *EMBO Rep.* **15**, 282-290.

Kuijt, T. E., Omerzu, M., Saurin, A. T. and Kops, G. J. (2014). Conditional targeting of MAD1 to kinetochores is sufficient to reactivate the spindle assembly checkpoint in metaphase. *Chromosoma*.

Laurell, E., Beck, K., Krupina, K., Theerthagiri, G., Bodenmiller, B., Horvath, P., Aebersold, R., Antonin, W. and Kutay, U. (2011). Phosphorylation of Nup98 by multiple kinases is crucial for NPC disassembly during mitotic entry. *Cell* **144**, 539-550.

Lee, S. H., Sterling, H., Burlingame, A. and McCormick, F. (2008). Tpr directly binds to Mad1 and Mad2 and is important for the Mad1-Mad2-mediated mitotic spindle checkpoint. *Genes Dev.* **22**, 2926-2931.

Lewis, J. D. and Tollervey, D. (2000). Like attracts like: getting RNA processing together in the nucleus. *Science* **288**, 1385-1389.

Li, Y. and Benezra, R. (1996). Identification of a human mitotic checkpoint gene: hsMAD2. *Science* **274**, 246-248.

Li, Y., Gorbea, C., Mahaffey, D., Rechsteiner, M. and Benezra, R. (1997). MAD2 associates with the cyclosome/anaphase-promoting complex and inhibits its activity. *Proc. Natl. Acad. Sci. USA* **94**, 12431-12436.

Lince-Faria, M., Maffini, S., Orr, B., Ding, Y., Cláudia Florindo, Sunkel, C. E., Tavares, A., Johansen, J., Johansen, K. M. and Maiato, H. (2009). Spatiotemporal control of mitosis by the conserved spindle matrix protein Megator. *J. Cell Biol.* **184**, 647-657.

London, N. and Biggins, S. (2014). Mad1 kinetochore recruitment by Mps1-mediated phosphorylation of Bub1 signals the spindle checkpoint. *Genes Dev.* **28**, 140-152.

Lusk, C. P., Waller, D. D., Makhnevych, T., Dienemann, A., Whiteway, M., Thomas, D. Y. and Wozniak, R. W. (2007). Nup53p is a target of two mitotic kinases, Cdk1p and Hrr25p. *Traffic* **8**, 647-660.

Ma, H. T. and Poon, R. Y. (2011). How protein kinases co-ordinate mitosis in animal cells. *Biochem. J.* **435**, 17-31.

Macaulay, C., Meier, E. and Forbes, D. J. (1995). Differential mitotic phosphorylation of proteins of the nuclear pore complex. *J. Biol. Chem.* **270**, 254-262.

Makhnevych, T., Lusk, C. P., Anderson, A. M., Aitchison, J. D. and Wozniak, R. W. (2003). Cell cycle regulated transport controlled by alterations in the nuclear pore complex. *Cell* **115**, 813-823.

Mansfeld, J., Güttinger, S., Hawryluk-Gara, L. A., Panté, N., Mall, M., Galy, V., Haselmann, U., Mühlhäusser, P., Wozniak, R. W., Mattaj, I. W. et al. (2006). The conserved transmembrane nucleoporin NDC1 is required for nuclear pore complex assembly in vertebrate cells. *Mol. Cell* **22**, 93-103.

Miller, M. W., Caracciolo, M. R., Berlin, W. K. and Hanover, J. A. (1999). Phosphorylation and glycosylation of nucleoporins. *Arch. Biochem. Biophys.* **367**, 51-60.

Moyle, M. W., Kim, T., Hattersley, N., Espeut, J., Cheerambathur, D. K., Oegema, K. and Desai, A. (2014). A Bub1-Mad1 interaction targets the Mad1-Mad2 complex to unattached kinetochores to initiate the spindle checkpoint. *J. Cell Biol.* **204**, 647-657.

Mühlhäusser, P. and Kutay, U. (2007). An in vitro nuclear disassembly system reveals a role for the RanGTPase system and microtubule-dependent steps in nuclear envelope breakdown. *J. Cell Biol.* **178**, 595-610.

Nakano, H., Funasaka, T., Hashizume, C. and Wong, R. W. (2010). Nucleoporin translocated promoter region (Tpr) associates with dynein complex, preventing chromosome lagging formation during mitosis. *J. Biol. Chem.* **285**, 10841-10849.

Niepel, M., Strambio-de-Castillia, C., Fasolo, J., Chait, B. T. and Rout, M. P. (2005). The nuclear pore complex-associated protein, Mlp2p, binds to the yeast spindle pole body and promotes its efficient assembly. *J. Cell Biol.* **170**, 225-235.

Nigg, E. A. (1990). Mechanisms of signal transduction to the cell nucleus. *Adv. Cancer Res.* **55**, 271-310.
Nigg, E. A. (1997). Nucleocytoplasmic transport: signals, mechanisms and regulation. *Nature* **386**, 779-787.
Nousiainen, M., Silljé, H. H., Sauer, G., Nigg, E. A. and Körner, R. (2006). Phosphoproteome analysis of the human mitotic spindle. *Proc. Natl. Acad. Sci. USA* **103**, 5391-5396.
Obenauer, J. C., Cantley, L. C. and Yaffe, M. B. (2003). Scansite 2.0: Proteome-wide prediction of cell signaling interactions using short sequence motifs. *Nucleic Acids Res.* **31**, 3635-3641.
Olson, M. O., Dundr, M. and Szebeni, A. (2000). The nucleolus: an old factory with unexpected capabilities. *Trends Cell Biol.* **10**, 189-196.
Onischenko, E. A., Gubanova, N. V., Kiseleva, E. V. and Hallberg, E. (2005). Cdk1 and okadaic acid-sensitive phosphatases control assembly of nuclear pore complexes in Drosophila embryos. *Mol. Biol. Cell* **16**, 5152-5162.
Pederson, T. (1998). The plurifunctional nucleolus. *Nucleic Acids Res.* **26**, 3871-3876.
Pemberton, L. F. and Paschal, B. M. (2005). Mechanisms of receptor-mediated nuclear import and nuclear export. *Traffic* **6**, 187-198.
Petronczki, M., Lénárt, P. and Peters, J. M. (2008). Polo on the Rise-from Mitotic Entry to Cytokinesis with Plk1. *Dev. Cell* **14**, 646-659.
Portier, N., Audhya, A., Maddox, P. S., Green, R. A., Dammermann, A., Desai, A. and Oegema, K. (2007). A microtubule-independent role for centrosomes and aurora a in nuclear envelope breakdown. *Dev. Cell* **12**, 515-529.
Rajanala, K. and Nandicoori, V. K. (2012). Localization of nucleoporin Tpr to the nuclear pore complex is essential for Tpr mediated regulation of the export of unspliced RNA. *PLoS ONE* **7**, e29921.
Raška, I., Shaw, P. J. and Cmarko, D. (2006). Structure and function of the nucleolus in the spotlight. *Curr. Opin. Cell Biol.* **18**, 325-334.
Santamaria, A., Wang, B., Elowe, S., Malik, R., Zhang, F., Bauer, M., Schmidt, A., Sillje, H. H., Korner, R. and Nigg, E. A. (2011). The Plk1-dependent phosphoproteome of the early mitotic spindle. *Mol. Cell Proteomics* **10**, M110 004457.
Schneider, R. and Grosschedl, R. (2007). Dynamics and interplay of nuclear architecture, genome organization, and gene expression. *Genes Dev.* **21**, 3027-3043.
Schneider, C. A., Rasband, W. S. and Eliceiri, K. W. (2012). NIH Image to ImageJ: 25 years of image analysis. *Nat. Methods* **9**, 671-675.
Schweizer, N., Ferrás, C., Kern, D. M., Logarinho, E., Cheeseman, I. M. and Maiato, H. (2013). Spindle assembly checkpoint robustness requires Tpr-mediated regulation of Mad1/Mad2 proteostasis. *J. Cell Biol.* **203**, 883-893.
Shibata, S., Matsuoka, Y. and Yoneda, Y. (2002). Nucleocytoplasmic transport of proteins and poly(A)+ RNA in reconstituted Tpr-less nuclei in living mammalian cells. *Genes Cells* **7**, 421-434.
Shou, W., Seol, J. H., Shevchenko, A., Baskerville, C., Moazed, D., Chen, Z. W., Jang, J., Shevchenko, A., Charbonneau, H. and Deshaies, R. J. (1999). Exit from mitosis is triggered by Tem1-dependent release of the protein phosphatase Cdc14 from nucleolar RENT complex. *Cell* **97**, 233-244.
Tahara, K., Takagi, M., Ohsugi, M., Sone, T., Nishiumi, F., Maeshima, K., Horiuchi, Y., Tokai-Nishizumi, N., Imamoto, F., Yamamoto, T. et al. (2008). Importin-beta and the small guanosine triphosphatase Ran mediate chromosome loading of the human chromokinesin Kid. *J. Cell Biol.* **180**, 493-506.
Tao, W. and Levine, A. J. (1999). P19(ARF) stabilizes p53 by blocking nucleo-cytoplasmic shuttling of Mdm2. *Proc. Natl. Acad. Sci. USA* **96**, 6937-6941.
Terry, L. J., Shows, E. B. and Wente, S. R. (2007). Crossing the nuclear envelope: hierarchical regulation of nucleocytoplasmic transport. *Science* **318**, 1412-1416.
Visintin, R. and Amon, A. (2000). The nucleolus: the magician's hat for cell cycle tricks. *Curr. Opin. Cell Biol.* **12**, 372-377.
Visintin, R., Hwang, E. S. and Amon, A. (1999). Cfi1 prevents premature exit from mitosis by anchoring Cdc14 phosphatase in the nucleolus. *Nature* **398**, 818-823.
Vomastek, T., Iwanicki, M. P., Burack, W. R., Tiwari, D., Kumar, D., Parsons, J. T., Weber, M. J. and Nandicoori, V. K. (2008). Extracellular signal-regulated kinase 2 (ERK2) phosphorylation sites and docking domain on the nuclear pore complex protein Tpr cooperatively regulate ERK2-Tpr interaction. *Mol. Cell. Biol.* **28**, 6954-6966.
Weber, J. D., Taylor, L. J., Roussel, M. F., Sherr, C. J. and Bar-Sagi, D. (1999). Nucleolar Arf sequesters Mdm2 and activates p53. *Nat. Cell Biol.* **1**, 20-26.
Wen, W., Meinkoth, J. L., Tsien, R. Y. and Taylor, S. S. (1995). Identification of a signal for rapid export of proteins from the nucleus. *Cell* **82**, 463-473.
Wu, J., Matunis, M. J., Kraemer, D., Blobel, G. and Coutavas, E. (1995). Nup358, a cytoplasmically exposed nucleoporin with peptide repeats, Ran-GTP binding sites, zinc fingers, a cyclophilin A homologous domain, and a leucine-rich region. *J. Biol. Chem.* **270**, 14209-14213.
Yang, C., Hao, J., Kong, D., Cui, X., Zhang, W., Wang, H., Guo, X., Ma, S., Liu, X., Pu, P. and Xu, B. (2014). ATM-mediated Mad1 Serine 214 phosphorylation regulates Mad1 dimerization and the spindle assembly checkpoint. *Carcinogenesis.* [E-pub ahead of print].
Yoon, S. O., Shin, S., Liu, Y., Ballif, B. A., Woo, M. S., Gygi, S. P. and Blenis, J. (2008). Ran-binding protein 3 phosphorylation links the Ras and PI3-kinase pathways to nucleocytoplasmic transport. *Mol. Cell* **29**, 362-375.
Zimowska, G. and Paddy, M. R. (2002). Structures and dynamics of Drosophila Tpr inconsistent with a static, filamentous structure. *Exp. Cell Res.* **276**, 223-232.